

# Source apportionment of wide range particle size spectra and black carbon collected at the airport of Venice (Italy)

Masiol, Mauro; Vu, Tuan V.; Beddows, David; Harrison, Roy

DOI:

[10.1016/j.atmosenv.2016.05.018](https://doi.org/10.1016/j.atmosenv.2016.05.018)

License:

Creative Commons: Attribution-NonCommercial-NoDerivs (CC BY-NC-ND)

*Document Version*

Peer reviewed version

*Citation for published version (Harvard):*

Masiol, M, Vu, TV, Beddows, D & Harrison, R 2016, 'Source apportionment of wide range particle size spectra and black carbon collected at the airport of Venice (Italy)', *Atmospheric Environment*, vol. 139, pp. 56-74.  
<https://doi.org/10.1016/j.atmosenv.2016.05.018>

[Link to publication on Research at Birmingham portal](#)

**Publisher Rights Statement:**

Checked May 2016

**General rights**

Unless a licence is specified above, all rights (including copyright and moral rights) in this document are retained by the authors and/or the copyright holders. The express permission of the copyright holder must be obtained for any use of this material other than for purposes permitted by law.

- Users may freely distribute the URL that is used to identify this publication.
- Users may download and/or print one copy of the publication from the University of Birmingham research portal for the purpose of private study or non-commercial research.
- User may use extracts from the document in line with the concept of 'fair dealing' under the Copyright, Designs and Patents Act 1988 (?)
- Users may not further distribute the material nor use it for the purposes of commercial gain.

Where a licence is displayed above, please note the terms and conditions of the licence govern your use of this document.

When citing, please reference the published version.

**Take down policy**

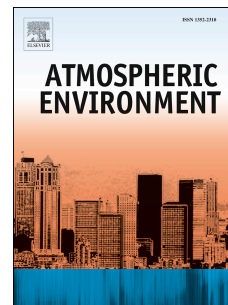
While the University of Birmingham exercises care and attention in making items available there are rare occasions when an item has been uploaded in error or has been deemed to be commercially or otherwise sensitive.

If you believe that this is the case for this document, please contact [UBIRA@lists.bham.ac.uk](mailto:UBIRA@lists.bham.ac.uk) providing details and we will remove access to the work immediately and investigate.

# Accepted Manuscript

Source apportionment of wide range particle size spectra and black carbon collected at the airport of Venice (Italy)

Mauro Masiol, Tuan V. Vu, David C.S. Beddows, Roy M. Harrison



PII: S1352-2310(16)30359-4

DOI: [10.1016/j.atmosenv.2016.05.018](https://doi.org/10.1016/j.atmosenv.2016.05.018)

Reference: AEA 14606

To appear in: *Atmospheric Environment*

Received Date: 18 November 2015

Revised Date: 6 May 2016

Accepted Date: 9 May 2016

Please cite this article as: Masiol, M., Vu, T.V., Beddows, D.C.S., Harrison, R.M., Source apportionment of wide range particle size spectra and black carbon collected at the airport of Venice (Italy), *Atmospheric Environment* (2016), doi: 10.1016/j.atmosenv.2016.05.018.

This is a PDF file of an unedited manuscript that has been accepted for publication. As a service to our customers we are providing this early version of the manuscript. The manuscript will undergo copyediting, typesetting, and review of the resulting proof before it is published in its final form. Please note that during the production process errors may be discovered which could affect the content, and all legal disclaimers that apply to the journal pertain.

1  
2  
3  
4  
5  
6 **SOURCE APPORTIONMENT OF WIDE**  
7 **RANGE PARTICLE SIZE SPECTRA AND**  
8 **BLACK CARBON COLLECTED AT THE**  
9 **AIRPORT OF VENICE (ITALY)**  
10

11  
12 **Mauro Masiol, Tuan V. Vu, David C.S. Beddows and**  
13 **Roy M. Harrison<sup>\*†</sup>**  
14

15  
16 **Division of Environmental Health and Risk Management**  
17 **School of Geography, Earth and Environmental Sciences**  
18 **University of Birmingham**  
19 **Edgbaston, Birmingham B15 2TT**  
20 **United Kingdom**  
21  
22  
23

---

\* To whom correspondence should be addressed.

Tele: +44 121 414 3494; Fax: +44 121 414 3708; Email: r.m.harrison@bham.ac.uk

†Also at: Department of Environmental Sciences / Center of Excellence in Environmental Studies, King Abdulaziz University, PO Box 80203, Jeddah, 21589, Saudi Arabia

**HIGHLIGHTS**

- 24
- 25 ➤ Particle number, size and black carbon were measured at the airport of Venice
- 26 ➤ Data were analysed along with gases, weather parameters and flight traffic
- 27 ➤ Six potential sources were identified and apportioned by PMF analysis on PNSD
- 28 ➤ Airport emissions contributed ~20% to the total PNC
- 29 ➤ No specific local sources of BC can be identified as dominant

30

31

32

33

34

35

36

37

38

39

40

41

42

43

44

45

46

47

48

49

50

51 **ABSTRACT**

52 Atmospheric particles are of high concern due to their toxic properties and effects on climate, and  
53 large airports are known as significant sources of particles. This study investigates the contribution  
54 of the Airport of Venice (Italy) to black carbon (BC), total particle number concentrations (PNC)  
55 and particle number size distributions (PNSD) over a large range (14 nm to 20  $\mu\text{m}$ ). Continuous  
56 measurements were conducted between April and June 2014 at a site located 110 m from the main  
57 taxiway and 300 m from the runway. Results revealed no significantly elevated levels of BC and  
58 PNC, but exhibited characteristic diurnal profiles. PNSD were then analyzed using both *k*-means  
59 cluster analysis and positive matrix factorization. Five clusters were extracted and identified as  
60 midday nucleation events, road traffic, aircraft, airport and nighttime pollution. Six factors were  
61 apportioned and identified as probable sources according to the size profiles, directional  
62 association, diurnal variation, road and airport traffic volumes and their relationships to  
63 micrometeorology and common air pollutants. Photochemical nucleation accounted for ~44% of  
64 total number, followed by road+shipping traffic (26%). Airport-related emissions accounted for  
65 ~20% of total PNC and showed a main mode at 80 nm and a second mode beyond the lower limit of  
66 the SMPS (<14 nm). The remaining factors accounted for less than 10% of number counts, but were  
67 relevant for total volume concentrations: nighttime nitrate, regional pollution and local  
68 resuspension. An analysis of BC levels over different wind sectors revealed no especially  
69 significant contributions from specific directions associated with the main local sources, but a  
70 potentially significant role of diurnal dynamics of the mixing layer on BC levels. The approaches  
71 adopted in this study have identified and apportioned the main sources of particles and BC at an  
72 international airport located in area affected by a complex emission scenario. The results may  
73 underpin measures for improving local and regional air quality, and health impact assessment  
74 studies.

75

76 **Keywords:** Airport; black carbon; size distributions; source apportionment; ultrafine particles

77

78 **1. INTRODUCTION**

79 Ambient air pollution, particularly airborne particulate matter (PM), exerts a large influence on  
80 public opinion and with policy-makers and the scientific community because of its known adverse  
81 effects on human health (Heal et al., 2012; Beelen et al., 2014) and its complex implications for  
82 climate (Kulmala et al., 2011; Fiore et al., 2012). The transformation and combustion of fossil fuels  
83 are amongst the main sources worldwide impacting upon PM and are studied widely because of the  
84 increasing demand for energy driven by industrialised countries and the economic growth of  
85 emerging regions. Besides the well-recognised sources which combust fossil fuels (e.g., road traffic,  
86 shipping, industries, domestic heating), aviation deserves particular attention because of the rapid  
87 growth of civil aviation. Despite the occurrence of events of global impact, such as the terrorist  
88 attack of 11th September 2011, the outbreak of severe acute respiratory syndrome in 2002–2003  
89 and the recent global economic crisis (2008–2009), civil aviation has experienced an almost  
90 constant growth from the 1930s to present day. This trend (about +5% every year) is expected to  
91 continue over the next decades (Lee et al., 2009).

92

93 The global-scale impacts of civil aviation are heavily debated and are principally attributed to the  
94 climate forcing of exhausts emitted at cruising altitudes. In the lower troposphere, civil aviation has  
95 more local effects, which are mainly attributed to the noise and the deterioration of air quality at  
96 ground-level due to airport operations. Up to today, many studies have been reported on aircraft  
97 engine exhaust emissions (Masiol and Harrison, 2014 and references therein), and emission  
98 standards for new types of aircraft engine have been implemented since the late 1970s for carbon  
99 monoxide (CO), nitrogen oxides ( $\text{NO}_x = \text{NO} + \text{NO}_2$ ), unburned hydrocarbons and smoke number  
100 (ICAO, 2008).

101

102 However, beside aircraft engine exhausts, other sources may affect air quality around airports, e.g.  
103 non-exhaust emissions from aircraft, emissions from the units providing power to the aircraft on the  
104 ground, the traffic due to the airport ground service, maintenance work, heating facilities, fugitive  
105 vapours from refuelling, transportation systems and road traffic for moving people and goods in and  
106 out of the airport. Beyond this complex emission scenario, most large airports are also located near  
107 heavily populated urban areas and are responsible for the build-up of some pollutants and  
108 exceedence of some air quality standards.

109

110 The Marie Skłodowska-Curie project CHEERS (Chemical and Physical Properties and Source  
111 Apportionment of Airport Emissions in the context of European Air Quality Directives) was  
112 motivated by the lack of information regarding the impacts of airports located near large cities. In  
113 particular, the role of airport emissions on the black carbon (BC), particle number concentration  
114 (PNC) and particle number size distributions (PNSD) are still debated, although some previous  
115 studies have provided evidence that aircraft are major sources of such pollutants. For example,  
116 Dodson et al. (2009) found that aircraft activity in close proximity to a small regional airport  
117 contributed 24–28% of the total BC measured at five sites 0.16–3.7 km from the airfield; Hudda et  
118 al. (2014) concluded that emissions from the Los Angeles international airport increase PNC 4-fold  
119 at 10 km downwind; Keuken et al. (2015) reported that the PNSD in an area affected by emissions  
120 from Schiphol airport (The Netherlands) was dominated by ultrafine (10 to 20 nm) particles.

121

122 This study aims to investigate the impacts of on-airport emissions on the levels of BC, PNC and  
123 PNSD over a very wide range (14 nm to 20  $\mu$ m) at a runway/taxiway-side site of the Marco Polo  
124 international airport (VCE). The airport is located ~5.5 km N to the historic city centre of Venice  
125 and ~6 km NE to the large urban area of Mestre (~270,000 inhabitants). This is an area  
126 characterised by many strong local anthropogenic pressures and a Mediterranean climate.

127

128 Among the well-established source apportionment methods, cluster analysis and receptor modelling  
129 techniques have been widely applied for characterising the PNSD and the most probable sources of  
130 airborne particles (e.g., Dall'Osto et al., 2012). Among the cluster analyses, *k*-means is the most  
131 widely used technique. Salimi et al. (2014) tested various clustering methods on PNSD data and  
132 reported that *k*-means resulted in a highest performance among others. Many studies have  
133 successfully applied *k*-means clustering for purposes similar to this study and under weather  
134 conditions comparable to N Italy: for example, Wegner et al. (2012) studied the characteristic size  
135 distributions in urban background environments; Brines et al. (2014; 2015) categorized PNSD  
136 measured in high-insolation cities (Barcelona, Madrid, Rome, Brisbane and Los Angeles), i.e. under  
137 weather conditions comparable to Venice; Beddows et al. (2014) explored the variations in  
138 tropospheric submicron particle size distributions all across Europe.

139

140 Among the receptor modelling techniques, positive matrix factorization (PMF) has been applied to  
141 PNSD data: Friend et al. (2013) compared the application of PMF and absolute principal  
142 component scores (PCA-APCS) for resolving sources of PNSD along a traffic corridor and  
143 concluded that PMF results were more reliable; Ogulei et al. (2007) modelled the source  
144 contributions to submicron PNSD measured in Rochester, NY, USA; Harrison et al. (2011) used  
145 PMF to quantify the sources of wide size spectra PNSD in the vicinity of a highway.

146

147 In this study, particle spectra were used as input for a *k*-means cluster analysis and a PMF receptor  
148 model aiming to characterise the PNSD and identify and quantify the main potential sources of  
149 particles, respectively. Data were also analysed jointly with common air pollutants, weather  
150 parameters and traffic profiles of airport and road traffic to investigate potential sources and  
151 formation mechanisms. Furthermore, an analysis of BC levels associated with different wind sectors  
152 allowed extraction of information on sources of soot particles and pointed out the effects of mixing  
153 layer dynamics on driving the levels of some pollutants in the study area.



## 154 2. MATERIALS AND METHODS

### 155 2.1 Site Description

156 Amongst other regions, the Po Valley (Northern Italy) represents one of the few remaining hotspots  
157 in Europe, where the levels of air pollutants (mainly NO<sub>2</sub>, PM<sub>10</sub> and PM<sub>2.5</sub>) are currently breaching  
158 the *target* or *limit* values imposed by European Directives. For this reason, the study of the main  
159 PM sources in the Po Valley is fundamental and VCE (Figure 1) represents an interesting case study  
160 for a number of reasons:

- 161 • it is the third airport of Italy for flight traffic with more than 100,000 annual aircraft  
162 movements. The major type of aircraft flying at VCE are short- to medium-range, narrow-body,  
163 twin-engine airliners: A320> A319> A321> B737-800 > B717;
- 164 • it is located close to a densely populated urban area (Mestre), where the levels of particulate  
165 matter pollution do not fully comply with the EC limit and target values (Masiol et al., 2014a);
- 166 • it is located in a coastal area and is therefore affected by the atmospheric circulation associated  
167 with sea/land breezes during the warm season. This circulation may potentially advect the  
168 pollutants emitted at the airport toward the mainland during the daytime;
- 169 • being located on the eastern edge of the Po Valley, it is potentially affected by the transport of  
170 pollutants at regional or even transboundary scales (e.g., Squizzato and Masiol, 2015);
- 171 • the air quality scenario of the area is extremely complex because of the high range of differing  
172 potential sources, including: (1) high density residential areas mostly using methane for  
173 domestic heating, even though the burning of wood (i.e. logs, briquettes, chips and pellets) is  
174 nowadays becoming an increasing alternative; (2) heavily trafficked roads which are highly  
175 congested during peak hours with light and heavy duty vehicles using gasoline, diesel and LPG  
176 fuels; (3) a motorway and a motorway-link which are a part of the main European routes E55  
177 and E70, with the consequent heavy duty vehicle traffic transporting goods between Italy,  
178 Eastern and Central Europe; (4) an extended industrial area (Porto Marghera) hosting a large  
179 number of different installations, including thermal power plants burning coal, gas and refuse

180 derived fuels, a large shipbuilding industry, oil-refinery, municipal solid waste incinerators and  
181 many other chemical, metallurgical and glass plants; (5) the artistic glassmaking factories in the  
182 Island of Murano, which is made up of small and medium-sized glassworks without significant  
183 measures for emission abatement; (6) heavy shipping traffic due to public transport,  
184 commercial and cruise terminals (annually, 3600–4000 vessels pass throughout the harbour of  
185 Venice accounting for a total tonnage of more than 25 billion kg);

- 186 • A preliminary study (Valotto et al., 2014) has indicated a potential influence of airport  
187 emissions on  $PM_{10}$  mass concentrations, mainly attributed to tyre wear during landing.

188

189 The site was set in an airport apron area at ca. 110 m from the main taxiway and ca. 300 m from the  
190 runway. The sampling site location (Figure 1) was the best compromise between stringent safety  
191 measures for flights and scientific purposes. Sea breezes occur during daytime approx. from April  
192 to October and blow air masses from the Adriatic Sea to the mainland (Figure SI1). Aircraft mostly  
193 used the runway 04L (landing and takeoff direction predominantly from SW to NE). During the  
194 sampling campaign, ~300 aircraft used the runway 22R (opposite direction to 04L, from NE to SW)  
195 out of a total of ~9500 flight movements (~3.2%). Under such circumstances, the site was chosen to  
196 catch the aircraft plumes and was set in a place downwind of the latter part of the taxiway and the  
197 beginning of the runway, where aircraft run their engines at 100% thrust during take-off or where  
198 the wheels hit the ground during landing causing smoke clearly visible to the naked eye. This  
199 choice was further supported by a modelling study (Pecorari et al., 2015) reporting that the site is  
200 affected by aircraft engine plumes for gaseous pollutants. A more detailed analysis of civil aviation  
201 traffic and wind direction is provided in Figure SI2: results indicate that a significant number of  
202 both takeoffs and landings occurred when the sampling site is downwind of the runway (winds from  
203 ~45°-160°).

204

205

206 **2.2 Instrumentation Suite**

207 An intensive sampling campaign was carried out from 28th April to 9th June 2014 at the VCE site.  
208 The period is representative of typical summer wind regimes (Figure S11), when air masses  
209 prevalently blow from NE at nighttime and from SSE during daytime. Ultrafine particle counts and  
210 their size distributions from 14.3 to 673.2 nm were measured at 5 min time resolution using a  
211 scanning mobility particle sizer spectrometer (SMPS) comprising a TSI 3080 electrostatic classifier,  
212 a TSI 3081 differential mobility analyzer (long DMA), a TSI 3087 X-ray aerosol neutraliser and a  
213 TSI 3022A condensation particle counter (CPC) based on *n*-butyl alcohol (Fisher Scientific, ACS)  
214 condensation. The range of size spectra were complemented by a TSI aerodynamic particle sizer  
215 (APS) 3321 which measures particle diameters within the range 0.5–19.8  $\mu\text{m}$ . BC was continuously  
216 measured in PM with aerodynamic diameter  $< 2.5 \mu\text{m}$  ( $\text{PM}_{2.5}$ ) with 5 min resolution using a 7-  
217 wavelength aethalometer (Magee Scientific AE31). Instrumental set-up: the SMPS operated at a  
218 sheath air to aerosol flow ratio of 10:1 (sheath and sample air flow rates were 3.0 and 0.3  $\text{L min}^{-1}$   
219 respectively, voltage 10-9591 V; density 1.2 g/cc; scan time 120 s, retrace 15 s; number of scan 2)  
220 while CPC operated at low flow rate (0.3  $\text{L min}^{-1}$ ). APS flow rate was 5  $\text{L min}^{-1}$ .

221  
222 Instruments were installed into a plastic/metal case over a stand and air inlets were ca. 2 m height  
223 and were composed of conductive materials to avoid particle losses and sampling artefacts. Devices  
224 were fully serviced, calibrated by authorised companies and underwent internal cross-calibrations  
225 with other similar instruments. Moreover, a periodic check and maintenance of instruments and  
226 cleaning of inlets was accomplished throughout the sampling campaign.

227  
228 Weather data including wind speed and direction, air temperature ( $^{\circ}\text{C}$ ), relative humidity (%RH),  
229 rain (mm), solar radiation ( $\text{W m}^{-2}$ ) and levels of some pollutants including  $\text{PM}_{2.5}$ , CO, ozone ( $\text{O}_3$ ),  
230 nitrogen oxides and sulphur dioxide ( $\text{SO}_2$ ) were also collected hourly at a nearby site (EZI site,  
231 Figure 1), which lies ~400 m from the site. Wind data were also collected at a sampling station

232 located in the industrial area (EZI5), which is indicative of the atmospheric circulation over the  
233 whole study area. Traffic data for both civil and general aviation including the type of aircraft, exact  
234 time of taxi-in, taxi-out, take-off and landing, were provided by the airport authorities. The profiles  
235 of traffic and urban emissions in the nearby urban area were derived from a previous study (Masiol  
236 et al., 2014b) which analysed 13 years of air pollution climate at an urban background site in  
237 Mestre.

238

### 239 **2.3 Data Handling and Chemometric Approaches**

240 Data were analysed using R version 3.1.2 (R Core Team, 2015). Preliminary data handling and  
241 clean-up were carried out to check the robustness of the dataset, detect anomalous records and to  
242 delete outliers. Data greater than the 99.5th percentile and negative values were removed from all  
243 the datasets while samples with unreliable behaviour were completely deleted. Missing bins of  
244 SMPS or APS data were replaced by linearly interpolated values from the nearest bins to that  
245 sample. Missing data for other variables were linearly interpolated between the nearest values of the  
246 time series.

247

248 In this study, 5-min resolution SMPS and APS spectra were used as input for clustering and PMF  
249 analyses. Size spectra were not merged, but a strategy was applied allowing use of raw data. In this  
250 way, unmerged spectra have been used also in previous source apportionment studies (e.g., Zhou et  
251 al., 2004; Ogulei et al., 2006). Input data were initially handled by averaging groups of three  
252 consecutive bins. This procedure has some advantages: (i) reduces the number of variables  
253 processed by the PMF, (ii) minimises the noise of raw SMPS data, which may cause high  
254 variability amongst consecutive bins and (iii) limits the number of null values (zeros) which are  
255 sometimes recorded in the more coarse bins of the SMPS and APS. This way, a total of 51 bins  
256 were used as input for PMF: 34 bins from the SMPS ranging from 14.6 nm to 552.3 nm and 17 bins  
257 from the APS (0.5–19.8  $\mu\text{m}$ ). In addition the total variable (total number of particles) was calculated

258 by summing the concentrations of each size bin adjusted with the appropriate multipliers accounting  
259 for channel resolutions of the SMPS and APS.

260

261 First, the PNSDs were grouped by applying a *k*-means cluster analysis. Details of the adopted  
262 method are provided in Beddows et al. (2009; 2014). Essentially, the methodology aims to group  
263 single PNSD spectra (SMPS+APS data, 5 min-resolved observations, in this case) into a number *k*  
264 of clusters. The partition of each observation into a cluster is based on the similarity of the PNSD  
265 spectra with the cluster centroids (means), i.e. the method is optimised to group similarly-shaped  
266 PNSD spectra into the same cluster. This strategy has the advantage to group observations with  
267 similar spectra, which are likely to be originated by the same set of emission sources or formation  
268 processes. The optimum number of clusters was determined by an optimisation algorithm based on  
269 the shape of the spectra (Beddows et al., 2009).

270

271 Subsequently, PMF analysis was performed on SMPS and APS data with 5 min resolution using the  
272 USEPA PMF 5 model. Details of the PMF model are reported elsewhere (Paatero and Tapper,  
273 1994; Paatero, 1997; USEPA, 2014; Hopke, 2016) and in supplementary material section SI1, while  
274 associated methods are well reviewed in Reff et al. (2007), Belis et al. (2014) and Brown et al.  
275 (2015). Uncertainty associated with the concentration data have been calculated by following a  
276 series of steps. Details are provided in supplementary material section SI2.

277

278 A series of R packages including ‘Openair’ (Carslaw and Ropkins, 2012) were additionally used to  
279 analyse some raw data, to link pollutant levels and PMF source contributions to the local  
280 atmospheric circulation and to detect the most probable local sources through bivariate polar plot  
281 analysis. Details of polar plots are given in Carslaw et al. (2006).

282

283

### 284 3. RESULTS AND DISCUSSION

#### 285 3.1 Overview of Data

286 The distribution of wind directions and the number of take-offs and landings in relation to the wind  
287 directions during the monitoring campaign are provided as supplementary material Figures SI1 and  
288 SI2, respectively. The wind roses during the sampling period and those for the warm season are  
289 similar, allowing extension of the results of this study to the whole period late spring-early fall.

290  
291 Results of all collected data are summarised as boxplots in Figure 2a. PNCs were split into 4  
292 ranges: nucleation (14-30 nm), Aitken nuclei (30 to 100 nm), accumulation (0.1 to 1  $\mu\text{m}$ ) and coarse  
293 (1 to 19.8  $\mu\text{m}$ ). On average the total PNC was  $\sim 1.4 \cdot 10^4$  particles  $\text{cm}^{-3}$ , of which  $7.3 \cdot 10^3$ ,  $4.3 \cdot 10^3$ ,  
294  $1.4 \cdot 10^3$  and 1.1 particles  $\text{cm}^{-3}$  were classified as nucleation, Aitken, accumulation and coarse  
295 ranges, respectively. The total PNC was comparable with particle concentrations normally observed  
296 in the Po Valley during summer (Rodríguez et al., 2005; Hamed et al., 2007). The highest average  
297 concentrations for other pollutants followed the order (in  $\mu\text{g m}^{-3}$ ): CO (474) > O<sub>3</sub> (76) > NO<sub>x</sub> (53) >  
298 NO<sub>2</sub> (47) > PM<sub>2.5</sub> (16) > NO (3.5) > BC (1.2) > SO<sub>2</sub> (0.8).

299  
300 Figure 2b shows the diurnal profiles of pollutants at local time, flight traffic and weather parameters  
301 computed by hourly averaging the data. Nucleation range particles show an evident increase during  
302 daytime, which is broadly comparable with the diurnal pattern in solar irradiance. Similar diurnal  
303 cycles have been observed in other studies (e.g., Kulmala and Kerminen, 2008; Chen et al., 2011;  
304 Hirsikko et al., 2013) and have been attributed to nucleation events driven by photochemical  
305 reactions and possibly assisted by turbulent mixing in the atmosphere (Janssen et al., 2012).  
306 However, the diurnal cycle of nucleation particles is also very similar to that of air traffic intensity.  
307 Aitken, accumulation and coarse particles, CO, nitrogen oxides and BC exhibit highest  
308 concentrations in the early morning and secondarily in the evening. These patterns are mainly  
309 driven by the interaction of emissions, dispersion and atmospheric chemical processes. Similar

310 diurnal cycles have been previously observed at an urban background site in Mestre-Venice for  
311 gaseous pollutants (Masiol et al., 2014b). Following the complex photochemistry of the NO-NO<sub>2</sub>-  
312 O<sub>3</sub> system, the cycle of O<sub>3</sub>, which show a daily peak in the afternoon, is the inverse of the cycle of  
313 traffic emissions. Despite the very low concentrations of SO<sub>2</sub> normally recorded over the study area,  
314 a daily cycle similar to ozone can be identified. Since the daylight hours of the warm season are  
315 characterized by the presence of sea breezes, an influence of the local circulation pattern on the  
316 levels of O<sub>3</sub> and SO<sub>2</sub> should be further considered. Figures 2b also shows the daily pattern of wind,  
317 showing highest speeds in the afternoon (average 3.5 m s<sup>-1</sup>), which are mainly caused by the  
318 influence of sea breezes.

319

320 Derived parameters are also show in Figure 2. The NO<sub>2</sub>/NO<sub>x</sub> ratio is indicative of the partitioning of  
321 nitrogen oxides. In Europe, despite the efforts to lower the NO<sub>x</sub> emissions, NO<sub>2</sub> levels do not yet  
322 meet the targets in many locations, including the study area. This is attributed to a discrepancy  
323 between achieving NO<sub>x</sub> emission reductions and NO<sub>2</sub> ambient concentrations (e.g., Grice et al.,  
324 2009; Cyrus et al., 2012), which has been related to the growing proportion of diesel-powered  
325 vehicles with known high primary (direct) emissions of NO<sub>2</sub> (Carslaw et al., 2007). In the study area  
326 (Province of Venice), the emission inventories for 2007/8 (ARPAV, 2014) indicated a cumulative  
327 emission of 24.4 Gg NO<sub>x</sub> y<sup>-1</sup>, mainly attributed to road transport (37%), combustion in energy and  
328 transformation industries (24%) and other mobile sources and machinery (21%). Airport emissions  
329 fall into this latter category: aircraft engines emit NO<sub>x</sub>, and emissions increase with engine thrust,  
330 i.e. are higher during take-off and lower in taxi and idle phases. The NO-NO<sub>2</sub> partitioning in the  
331 emissions of modern high by-pass turbofan engines is also thrust-dependent: NO<sub>2</sub> is principally  
332 emitted at idle, while NO is dominant at higher thrust regimes (Wormhoudt et al., 2007). At a first  
333 glance, the diurnal profile of NO<sub>2</sub>/NO<sub>x</sub> ratio can be related to airport emissions due to takeoffs  
334 (higher NO), however the daily pattern and value of the ratio are similar to those observed at an  
335 urban background site in Mestre-Venice (Masiol et al., 2014b), indicating that vehicular traffic is

336 probably the most influential source. The level of total oxidants ( $OX=O_3+NO_2$ , in ppbv) is useful to  
337 assess the oxidative potential in the atmosphere (Kley et al., 1999). Results show that OX levels are  
338 mainly driven by ozone and highest concentrations are recorded in the afternoon.

339

340 A preliminary investigation of the location of potential local sources of atmospheric pollutants was  
341 assessed by mean of polar plots (Figure 3) and polar annulus (Figure SI3) analysis. Polar plots  
342 essentially map the pollutant concentrations by wind speed and direction as a continuous surface  
343 (Carslaw and Ropkins, 2012). Polar annuli map the average levels of pollutants by wind direction  
344 and hours of the day. Generally, most air pollutants ( $NO$ ,  $NO_2$ ,  $OX$ ,  $SO_2$  and  $PNC$ ) show increasing  
345 average concentrations for winds blowing from the SE and SW quadrants,  $CO$  decreases for  
346 moderate winds from the South and stronger winds from NW, ozone shows no prevalent sector but  
347 increases with wind speed, while  $PM_{2.5}$  and  $BC$  increase in calm wind periods and for  
348 moderate/strong winds from E, W and S. In particular, some important insights into the location of  
349 potential sources can be extracted from the polar plot analysis:

- 350 •  $NO$  increases towards the ESE, i.e. from the beginning of the runway, where aircraft generally  
351 stop and speed up the engines at full power before takeoff. This finding is also evident if  
352 considering the partitioning of  $NO_x$ , which shows a remarkable drop of  $NO_2/NO_x$  toward the  
353 runway, indicative of a local source. In addition,  $NO$  also increases toward the S-SW sector  
354 probably because of emissions of road traffic in Mestre and shipping in Venice;
- 355 • Despite its very low concentration,  $SO_2$  (an excellent tracer for shipping, aircraft and oil  
356 refineries) seems to be related more to industrial emissions (SW quadrant) and to the Port of  
357 Venice (SE), than to the airport activities (quadrant to NE);
- 358 •  $PNC$  increases toward the SE and SW quadrants, particularly for strong winds from the South,  
359 and to a minor extent, from the NE quadrant. These findings suggest that airport activities are not  
360 the main source of particles in the area;



361 •  $PM_{2.5}$  increases towards the East, South and West. Although increases from S and W can be  
362 related to external sources such as main roads and urban settlements, the high levels recorded  
363 towards the East, which roughly corresponds to the section of runway where planes generally  
364 land, may relate to aircraft emissions during landing.

365

366 In summary, even though the site was strategically located close to the runway and taxiway, the  
367 concurrent effects of multiple emission sources in the study area makes it difficult to assess the  
368 contribution made by the airport with simple polar plot analysis on raw data.

369

370 Figure 4 shows the median PNSDs calculated over the entire sampling campaign and categorised by  
371 time of day (01:00-07:00; 07:00-13:00; 13:00-19:00; 19:00-01:00 local time). Medians, 25th and  
372 75th percentiles for SMPS and APS data were then merged using the algorithm developed by  
373 Beddows et al. (2010), which also returns the particle volume concentrations (PVSDs). Results  
374 show a significant variation in diurnal modal structures of PNSDs with a main mode ranging from  
375 below 14 nm in the daytime periods to ~40-50 nm during nighttime and early morning. There are  
376 two main reasons for this results: (i) the increased airport activities (6am-10pm) emitting fresh  
377 nucleation particles, as reported by several studies (e.g., Anderson et al., 2005; Kinsey et al., 2010;  
378 Mazaheri et al., 2013) and (ii) the potential role of nucleation processes during daytime. In this  
379 latter context, the diurnal occurrence of sea breezes cannot be disregarded since it may have a  
380 potential role in transporting fresh air masses from the Adriatic Sea and the nearby lagoon, which  
381 are affected by large tidal cycles and are known sources of aerosol precursor compounds. The  
382 production of secondary ultrafine particles may occur in the marine boundary layer by the  
383 nucleation of low vapour pressure gases produced naturally (but also of anthropogenic origin) (e.g.,  
384 O'Dowd and De Leeuw, 2007; Modini et al., 2009): through (1) homogeneous nucleation and (2)  
385 the subsequent particle growth via a number of mechanisms and scavenging of clusters by larger  
386 pre-existing particles. However, the diurnal variations may also be linked to the main (primary)

387 emission sources in the study area, i.e. mobile emissions either from road or maritime sources  
388 (commercial and tourist ships, private and public transport boats). On the contrary, PVSDs seem to  
389 undergo only modest changes throughout the day, with two main modes at 300-400 nm and 3-5  $\mu\text{m}$ .

390

### 391 **3.2 *k*-means cluster analysis**

392 Five clusters were extracted by the optimisation algorithm ( $k=5$ ). From a mathematical point of  
393 view,  $k=5$  returns optimal parameters (Figure SI4), i.e. a local maximum in the Dunn indices  
394 (0.0017) and a silhouette width of 0.43 (Beddows et al., 2009).  $k=5$  is also a good compromise for  
395 interpretation of PNSD spectra observations from a practical point of view. Hussein et al. (2014)  
396 have reported that is not prudent to describe the PNSD with either too few or too many clusters: few  
397 clusters (2–4) are not enough to explain variations and detailed differences in the particle number  
398 size distributions observed in the urban atmosphere, while extracting too many ( $> 10$ ) clusters may  
399 make the aerosol source attribution more challenging.

400

401 The centroids (means) of PNSD clusters are reported as solid lines in Figure 5 along with: (i) their  
402 10th, 25th, 75th and 90th percentile spectra as shaded areas; (ii) the volume size distributions  
403 (dashed line); (iii) the hourly counts and (iv) wind roses associated to each cluster. The number of  
404 observations in each cluster is reported in Figure SI4. Results show that diurnal count profiles are  
405 different for most of the clusters (although cluster 2 and 5 present similar hourly count profiles),  
406 while 3 clusters exhibit similar wind roses (cluster 2, 4, 5: winds from SE). To facilitate the  
407 interpretation of results, a series of 5 consecutive days (23th May 0:00 to 27th May 23:00) was  
408 selected and investigated in depth; the period was chosen to be representative of the typical cycling  
409 of clusters and typical meteorological conditions. Figure 6 reports a large number of variables  
410 measured within this period, including cluster number counts, airport movements  
411 (arrivals+departures), solar radiation, NO, SO<sub>2</sub>, and SMPS data (total PNC for nucleation, Aitken

412 and accumulation ranges and the contour plot of PNSD). Arrows indicating the wind speed and  
413 direction data also accompany the plots to help the interpretation of results.

414 Cluster 1 accounts for 26% of total clustered observations and presents two distinct peaks: while the  
415 finest peak extends beyond the SMPS detection limit (14 nm), the other one is at 25-40 nm. It  
416 exhibits a diurnal profile compatible with road traffic, i.e. showing a morning (6-8am) and an  
417 evening (5-7pm) rush hour peak and its wind rose shows no dominant wind direction. From Figure  
418 6, it can be noted that observations belonging to cluster 1 may be consecutively dominant for  
419 several hours (e.g., 23th May from noon to midnight or 26th May from 6am to 6pm) irrespective of  
420 the prevailing wind direction. This finding is compatible with sources present all over the study  
421 area. All these insights seem to support its interpretation as traffic-related, i.e. observations with a  
422 strong influence of the road traffic emissions.

423  
424 Cluster 3 accounts for most of observations (29%), mainly measured overnight. Its spectrum  
425 presents a single well defined peak at approx. 50 nm and its wind rose exhibits the typical nighttime  
426 atmospheric circulation patterns (low NE winds). Figure 6 clearly shows that cluster 3 observations  
427 start to rise in number in the late evening (before midnight) and usually drop off to near-zero counts  
428 in the early morning (6-8am), while they are rarely recorded in the middle of the day. Consequently,  
429 cluster 3 can be interpreted as nighttime pollution, i.e. spectra affected by the rise of atmospheric  
430 pollutants due to the reduced height of the mixing layer and, probably, by the formation of  
431 nighttime nitrate due to the chemistry driving the heterogeneous reactions of  $N_2O_5$  and  $NO_3$  on  
432 aerosol surfaces (Seinfeld and Pandis, 2006; Bertram and Thornton, 2009; Brown and Stutz, 2012).

433  
434 Cluster 5 (14% of total observations) links spectra peaking at 20 nm and having maximum counts in  
435 the afternoon (noon-5pm) with a second minor peak in the morning rush hour (7am). Despite its  
436 diurnal profile and wind direction being compatible with the airport emissions, Figure 6 clearly  
437 shows that cluster 5 well depicts local nucleation events centred in the early afternoon. Daytime

438 nucleation events forming particles below 15 nm are often observed in coastal environments and are  
439 associated with high  $\cdot\text{OH}$  radical and  $\text{SO}_2$  concentrations, but also with iodine oxide gas-phase  
440 processes (O'Dowd et al., 1999; O'Dowd and Hoffmann, 2006). They are also widely observed at  
441 southern European sites without a nearby marine influence (Reche et al., 2011). At least 3  
442 nucleation events can be found over the selected period (23th, 24th and 27th May): they can be  
443 recognised from their typical “banana” shape (Figure 6). Midday nucleation events start at noon  
444 with a huge increment of PNC in the finest nucleation range and, then, particles generally continue  
445 to grow over the afternoon, evening and overnight to reach the Aitken and accumulation ranges.  
446 Most of the time, cluster 5 observations become dominant for several hours (generally from 4 to 8 h  
447 after the event), but the nucleation event generally lasts less than 24 hours.

448

449 PNSD spectra and clustering results were further investigated to detect and quantify the number of  
450 midday nucleation events during the sampling campaign. Despite the complexity of the emission  
451 scenario in VCE, a method similar to Dal Maso et al. (2005) was adopted. Data were visually  
452 analysed on a daily basis and midday nucleation events are then identified following well defined  
453 criteria: (i) only days with a significant number of non-missing records were evaluated; (ii)  
454 nucleation episodes must have a clear boost in particle below 30 nm starting around noon; (iii) most  
455 of the spectra in an event must be categorised into the cluster 5; (iv) increases in cluster 5-spectra  
456 must prevail over a time span of hours; (v) particles must show signs of growth after an event has  
457 been initiated. Following such criteria, 7 events have been successfully recorded from a total of 17  
458 valid days (~40%).

459

460 Remaining clusters 2 and 4 both account for 15% of total observations and have similar wind roses  
461 (prevailing moderate winds from the E-S sector), which may be compatible with airport emissions.  
462 However, they present different PNSD spectra. Cluster 2 links spectra characterised by a particles in  
463 the nucleation range and peaking beyond the minimum detection diameter of the SMPS (14 nm),

464 while cluster 4 groups spectra show a primary mode at 60-100 nm and, secondarily, beyond 14 nm.  
465 Most of the literature reports that aircraft engine exhausts emit particles in the nucleation range  
466 (Kinsey et al., 2010; Mazaheri et al., 2013; Masiol and Harrison, 2014; Lobo et al., 2012;2015),  
467 however, some studies also report a second mode in the accumulation range (e.g., Mazaheri et al.,  
468 2009). Looking at the aircraft traffic provided by the airport, it is clear that the hourly counts of  
469 cluster 2 well relate with the aircraft movements (Figures 2 and SI2). On the contrary, hourly counts  
470 for cluster 4 are pretty constant through the day (Figure 5) and the wind rose also recorded counts  
471 for winds blowing from the NNE sector, i.e. toward the airport terminal and aircraft park areas. In  
472 this light, it can be hypothesized that cluster 2 represents fresh emissions from taking-off or landing  
473 aircraft, whereas, cluster 4 is more related to background levels of particles due to the taxi phases  
474 and operations at the gates.

475  
476 Cluster analysis has helped in identifying the main spectral shapes and their frequency over the  
477 sampling period. Results show that the spectra are mainly caused by direct emissions, e.g., road and  
478 airport traffic (clusters 1, 2) or atmospheric processes, e.g., mixing layer height and air temperature  
479 (cluster 3) and midday nucleation events (cluster 5). However, in an environment with very large  
480 anthropogenic influences like VCE, it is likely that spectra can be either influenced by single  
481 sources/processes or concurrently shaped by multiple sources. Consequently, PMF analysis may  
482 yield the most robust information on the probable sources.

483

### 484 **3.3 PMF Results**

485 Following the signal-to-noise criterion and known instrumental limits, three variables (12, 14.9 and  
486 18.4  $\mu\text{m}$  size bins) were excluded from the model, while five variables (0.5, 0.6, 0.7, 0.9 and 10  $\mu\text{m}$   
487 particles) were labelled as “weak” by tripling their uncertainties. Two additional variables (15.1 and  
488 16.8 nm) were categorised as weak because of showing high scaled residuals in preliminary runs;  
489 the total particle concentration was set as the total variable (weak). A total of 172 samples were

490 excluded as containing missing or incomplete data. A final matrix composed of 49 variables and  
491 4434 samples was then used as input for the PMF. The model was run several times by  
492 investigating solutions between 3 and 10 factors, by changing the extra modelling uncertainty  
493 option and by finding the most physically plausible result. Solutions of each preliminary run were  
494 investigated to avoid poorly/awfully resolved sources or unstable results by: (i) checking the model  
495 diagnostics; (ii) identifying factors having significant inter-factor correlations (Pearson  $r > 0.4$  at  
496  $p < 0.01$ ); (iii) minimising the sums of the squared differences between the scaled residuals for pairs  
497 of base runs.

498

499 A final 6-factor solution with 9.5% extra uncertainty was selected as the best compromise over the  
500 PMF diagnostic results and interpretation reliability for factors. Generally, solutions with less than 6  
501 factors returned many unresolved profiles; 7-factors had higher inter-factor correlations, while for  
502  $> 8$  factors solutions generated profiles with  $Q$  well below the expected (theoretical) value of the  
503 residual sum of squares  $Q_{exp}$  and/or no physical meaning. Convergence of the final PMF solution  
504 was then ensured over multiple runs for the 6-factor solution using a random starting seed. PMF  
505 results were carefully checked by investigating the base model displacement error estimation  
506 (DISP) and bootstrapping (BS) error estimation (Paatero et al., 2014; Brown et al., 2015).

507 Diagnostics reported that: (i) no factor swaps occurred for DISP analysis indicating that there are  
508 not significant rotational ambiguities and the solution is sufficiently robust to be used; (ii) factor  
509 mapping from the BS runs suggested that the BS uncertainties can be interpreted and the selected  
510 number of factors is appropriate. PMF rotational ambiguities were further assessed by varying the  
511 FPEAK value (Paatero et al. 2002) between -5 and 10 and checking the relative changes in  $Q$ , the  
512 total number of negative contributions and the G-space plots for edges. The more physically  
513 realistic and independent solutions were obtained for FPEAK= 2.5. Uncertainties of FPEAK-  
514 rotated solutions were finally estimated over  $n=200$  BS runs.

515

516 The extracted factor profiles are presented in Figure 7 as normalised number and volume fractions,  
517 while uncertainties of the final solution are shown in Figure SI5 as percentage of species sum with  
518 the associated uncertainty estimated by BS. A summary of PMF results is also provided in Table 1.

519

520 A first attempt to link PMF factors with airport traffic was carried out by computing Spearman  
521 correlations among factor contributions and real airport traffic movements (total, arrivals,  
522 departures) at 5 min resolution. Airport traffic was elaborated to return the more plausible number  
523 of aircraft movements every 5 min and takes in account the exact timing of each movement. Traffic  
524 data include the timings of landing and parking at the terminal (for arrivals) and the timings of  
525 departure from gates and take-off (for departures). This way, each movement was adjusted for the  
526 real time that each aircraft was moving. The dataset was also handled to maximise the signal of  
527 aircraft, i.e. selecting hours with high airport traffic (10am-9pm) and wind regimes blowing air  
528 masses from the taxiway and runway to the sampling site (45 to 170 degree). No one factor showed  
529 significant ( $p < 0.001$ ) strong ( $\rho > 0.6$ ) or even weak ( $0.35 < \rho < 0.6$ ) correlation with airport traffic. This  
530 result may be explained by a number of reasons: (i) airport emissions are complicated to model and  
531 predict due to the large number of different phases in the LTO cycles: even if it possible to know  
532 the exact time of each movement, it is difficult to predict the timing and the relative position of  
533 aircraft at different phases (e.g., the time spent by aircraft in the queue at the beginning of the  
534 runway was not recorded or when they are exactly upwind of the sampling site); (ii) although  
535 aircraft engines are expected to be the larger contributors to the air pollution at the airport, other  
536 sources may interfere by emitting particles with similar size distributions and, then, adding noise to  
537 the PMF results (e.g., the aircraft auxiliary power units (APU), which are small on-board turbines  
538 providing a source of electrical power and compressed air when aircraft are parked at the gate and  
539 sometimes during taxi); (iii) other strong sources are present in the study area; (iv) wind data are  
540 recorded hourly and then interpolated for obtaining 5 min time resolution, therefore unknown

541 discrepancies may occur between estimated and real wind data. This latter point was overcome by  
542 investigating 1 h-averaged traffic and PMF data, but correlations were still low for all of the factors.  
543  
544 Due to the inability to link PMF factors directly with aircraft movements, the interpretation of the  
545 extracted sources was principally based on the modal characteristics of the distributions and further  
546 post-processing analyses including: (1) the daily trends of factor contributions (Figure 8); (2) the  
547 investigation of the source directionality by means of polar plot and polar annulus analyses (Figure  
548 8); (3) the results of Spearman rank correlations ( $\rho$ ) with other measured pollutants (Table 2) and  
549 (4) cross-correlation functions (CCFs) among variables and calculated at  $\pm 24$  h lag time using  
550 hourly averaged data or with higher time resolution (5 min) and within  $\pm 3$  h lag time for PMF  
551 source contributions and BC data (Figure 9).

552  
553 The *first factor* includes most of the particles in the nucleation range ( $< 25$  nm), exhibits a sharp  
554 mode in the number distribution at 15-20 nm and makes the largest contribution to the total PNC  
555 (43.8%, confidence interval at 95% based on 200 BS runs (c.i.<sub>95</sub>) between 43.4 and 44.1%).  
556 However, its contribution to the volume distribution is  $\sim 1\%$ . This factor shows significant  
557 ( $p < 0.001$ ) but weak ( $0.35 < \rho < 0.6$ ) positive correlations with NO (but not NO<sub>2</sub>), OX, solar irradiance,  
558 air temperature and exhibits an evident diurnal variation peaking at 1 pm and higher levels during  
559 the afternoon. The polar plot analysis (Figure 8) indicates enhanced levels when winds blow from  
560 the SW and SE quadrants: whilst the increase from the SE quadrant arises for high wind speeds ( $> 5$   
561  $\text{m s}^{-1}$ ) towards the airfield, the increase in the SW quadrant occurs for lower speeds ( $3\text{--}5 \text{ m s}^{-1}$ ).  
562 The polar annulus analysis indicates that the higher concentrations are for winds blowing from S to  
563 SW at 12 noon-4pm. This behaviour is consistent with the location of several anthropogenic sources  
564 in the study area which can contribute to particles in the nucleation range, i.e. the road traffic in the  
565 urban area of Mestre (toward SW), the stack emissions from the industrial area (SW), shipping in  
566 Venice and its tourist harbour (S) and the airport activities and aircraft movements (SE). In this



567 context, particles peaking in the nucleation range have been observed for multiple anthropogenic  
568 sources: (i) fresh diesel engines (Shi and Harrison, 1999), (ii) diesel-equipped boats at high engine  
569 loads (Petzold et al., 2010), (iii) coal-fired power plants (Nielsen et al., 2002; Liu et al., 2010)  
570 aircraft (Anderson et al., 2005; Kinsey et al., 2010; Mazaheri et al., 2013; Lobo et al., 2015).  
571 However, particles in this size range may also originate from photochemically-driven nucleation  
572 processes. The profile for this factor relates well to the shapes grouped in the cluster 5 in the *k*-  
573 means cluster analysis (midday nucleation events). The polar plot for this factor (Figure 8) also  
574 shows the highest intensity in areas of the plot showing the lowest PM<sub>2.5</sub> concentrations (Figure 3).  
575 This is consistent with nucleation being favoured by a low condensation sink (Dall'Osto et al.,  
576 2013).

577

578 Beside the number of potential sources for this factor, the daily profile (Figure 8) shows a sharp  
579 peak at noon-2pm which is strongly related to the solar irradiance and well matches with the hourly  
580 counts of cluster 5, but also bears some similarity to aircraft movements (Figure 2) or road traffic  
581 rush hours. Aircraft takeoffs start before 6am, when the contribution of this factor is still low.  
582 Moreover, the maximum average values shown in the polar and annulus plots at noon-2pm are  
583 towards the SW, which is not consistent with a main origin from the airfield.

584

585 Results of a subsequent study give further insights for interpreting the first factor. A similar  
586 sampling campaign was carried out in July 2014 at a kerbside site in the urban area of Mestre using  
587 a similar set of instruments (SMPS, aethalometer). Preliminary results of this study are provided as  
588 supplementary material: Figure SI6 shows the map of the sampling location, while Figure SI7  
589 reports the “nucleation factor” extracted by applying PMF analysis to SMPS data. These results  
590 show an identical size distribution (particles peaking at 15-20 nm) with a similar daily pattern (main  
591 peak at noon-1pm followed by a second minor peak at 6-7am). However, the polar plot analysis  
592 significantly differs showing strong increases for winds blowing from the SE, i.e. the direction of

593 the industrial zone. Since the kerbside site is located 9.5 km WSW from VCE and weather  
594 conditions were very similar (summer sea/land breeze regime), an origin of factor 1 from airport  
595 activities is not consistent with the results. An origin from the industrial zone is plausible. As  
596 already reported, a large coal-fired power plant and a an oil refinery are located in the industrial  
597 area of Porto Marghera and both installations are potential sources of particles in the nucleation  
598 range (Nielsen et al., 2002; Liu et al., 2010; Cheung et al., 2012) and SO<sub>2</sub>. Emission inventories for  
599 2010 (ARPAV – Regione Veneto, 2015) reported that combustion in energy and transformation  
600 industries accounts for ~72% of total SO<sub>2</sub> emissions in the Venice Province. It has been reported  
601 that the probability of nucleation is increased by elevated SO<sub>2</sub> concentrations (e.g., Stanier et al.,  
602 2004) and a 13 year-long monitoring of airborne pollutants conducted in Mestre (Masiol et al.,  
603 2014b) reported evident peaks of SO<sub>2</sub> for winds blowing from the industrial zone. A large influence  
604 of oil refineries and/or coal-fired power plants upon the particle number concentrations in the  
605 nucleation range have been observed in many parts of the world (e.g., Stevens et al., 2012; Cheung  
606 et al., 2012; González and Rodríguez, 2013).

607

608 All of these insights support the interpretation of factor 1 as mainly driven by photochemical  
609 nucleation processes occurring in the atmosphere (Seinfeld and Pandis, 2006; Zhang et al., 2011)  
610 probably including gas-to-particle conversion of SO<sub>2</sub>. CCFs (Figure 9) well depict the relationship  
611 between this factor and solar irradiation: a short delay of the highest positive correlations at +1/+2 h  
612 lags may be attributed to the time needed for the growth of nucleated particles into the measured  
613 size range. However, beside its main probable origin from photochemical nucleation of SO<sub>2</sub>, the  
614 directional analysis (Figure 8) further suggests that this factor might also be also secondarily  
615 associated with locally-emitting primary anthropogenic sources.

616

617 Since the sampling site is located downwind of major combustion sources during sea breeze  
618 regimes, particles arising from the urban area are sampled on timescales of several minutes after

619 emission and, then, may undergo to a substantial evaporative shrinkage resulting in a shift toward  
620 smaller sizes. The condensation/evaporation/dilution processes have been demonstrated to be major  
621 mechanisms in altering aerosol size distributions after primary particles in the nucleation range are  
622 emitted in the atmosphere (Zhang et al., 2004; Harrison et al., 2016); this effect has been observed  
623 in heavily developed urban areas, such as London (Dall'Osto et al., 2011). In addition, the polar  
624 plot for factor 1 also shows minor increases towards the airfield for strong winds. The sulphur  
625 content in jet fuel is limited to 3000 ppm and is commonly reported within the range 300–1100 ppm  
626 (Masiol and Harrison, 2014, and reference therein), which is approximately 30-100 times higher  
627 than that for automotive fuels (<10 ppm). Consequently, aircraft emissions are a high potential  
628 source of SO<sub>2</sub> and may secondarily contribute to this factor under some particular circumstances.

629

630 The summary, although this factor could consist of a few distinct sources resulting in poorly  
631 resolved PMF solutions, its fingerprint remains similar for solutions of up to 10 factors,  
632 demonstrating its structural robustness and the lack of potential artefacts upon the PMF solution. As  
633 a consequence, the hypothesis of multiple-source attribution for nucleation particles is plausible and  
634 it is impossible to assign to a specific one with certainty. However, the temporal profile and the fact  
635 that the same source profile was found in another site in the area and affected by different emission  
636 scenarios is very consistent with a nucleation source driven by regional processes and the most  
637 significant sources of sulphur dioxide in the area.

638

639 The *second factor* is made up of ultrafine particles in the nucleation range (20 to 100 nm) with a  
640 clear mode at 35–40 nm for the number distribution, and which accounts for 25.5% (c.i.<sub>.95</sub> 25.3–25.9  
641 %) of particle number. Its contribution to the volume distribution is low (~5%) and peaks at 80 and  
642 500 nm. Several observations link this factor to road traffic: (i) correlation analysis shows  
643 significant moderate positive associations with NO<sub>2</sub> ( $\rho=0.44$ ) and BC ( $\rho=0.41$ ), which are  
644 pollutants primarily emitted by road traffic (mainly diesel); (ii) such correlations have maxima at 0

645 h lag, suggesting covariant sources (Figure 9); (iii) the diurnal variations reveal a typical cycle  
646 common to traffic-related sources (morning and evening rush traffic hours); (iv) the directional  
647 analysis shows increased levels when air masses move from the main populated sectors of the  
648 mainland, i.e. the urban area of Mestre (SW), and several main roads towards the N and (v) the  
649 factor profile very similar to the cluster 1 (road traffic) extracted by the *k*-mean cluster analysis. It is  
650 extensively reported that particles in the size range of factor 2 may originate from the dilution of  
651 diesel exhaust emissions (Charron and Harrison, 2003; Janhäll et al., 2004; Ntziachristos et al.,  
652 2007; Harrison et al., 2011) as well as from gasoline-powered cars (Wehner et al., 2009; Huang et  
653 al., 2013). Similar factor profiles have been also reported in the literature for road traffic (e.g., Yue  
654 et al., 2008; Constabile et al., 2009; Harrison et al., 2011).

655  
656 However, the polar plot analysis also shows increased levels for winds blowing from S, i.e. the  
657 direction of the historic city centre of Venice and its passenger terminal and for high wind regimes  
658 from SSE, i.e. toward the Lido inlet, a main entrance of cruise ships into the Lagoon of Venice. A  
659 number of studies have associated particles in this size range with marine traffic. Jonsson et al.  
660 (2011) reported that emissions from cargo and passenger ships peak at ~35 nm; Healy et al. (2009)  
661 observed ship exhaust particle number distributions with a maximum at approximately 50 nm;  
662 Kasper et al. (2007) observed mean diameters of particles at 20–40 nm for 2-stroke marine diesel  
663 engines; Petzold et al. (2010) associated particles with modes at 40–60 nm with a serial 4-stroke  
664 marine diesel engine at 10–50% engine load; Kivekäs et al. (2014) observed that the contribution of  
665 ship traffic to PNC downwind of a major shipping lane consists of number distributions peaking at  
666 ~40 nm. The same results were also reported by Lyyränen et al. (1999), who investigated the  
667 mechanisms of particle formation during combustion within marine diesel engines affected by hot  
668 corrosion and erosion. In the light of this, besides road traffic, factor 2 can be also linked to the  
669 marine traffic emissions from ships, waterbuses and boats of public or private transport services,  
670 which are commonly equipped with marine diesel engines. Currently, the contribution of the Port of

671 Venice to the levels of PM is heavily debated (Contini et al., 2015) and information on the  
672 emissions from waterbuses and the private boat fleet is still lacking (Pecorari et al., 2013a). Factor  
673 2 was interpreted as road+shipping traffic, mainly due to diesel engine emissions.

674

675 The *third factor* shows a main mode in the number distribution at 80 nm and a second mode in the  
676 nucleation range, which seems to extend beyond the lower limit of particle detection of the SMPS  
677 (14.6 nm). Three modes in the volume distribution are found at approx. 200, 500 nm and 5  $\mu\text{m}$ . Its  
678 contributions to the particle number and volume are 20.3% (c.i.<sub>0.95</sub> 20.1-20.5%) and 19.6%,  
679 respectively. This factor lacks relevant correlations with other air pollutants and its diurnal cycle is  
680 relatively constant through the early part of the day, with a strong decrease in the early afternoon  
681 following the increased wind speeds due to the sea breezes. Several studies available from the  
682 current literature report that aircraft engine emissions show a main mode in the nucleation range  
683 (Masiol and Harrison, 2014, and references therein; Lobo et al., 2015). However, despite the  
684 particle size profile of factor 3 differing from those commonly reported in the literature for aircraft  
685 emissions, there are a number of reasons for attributing this factor to the airport emissions:

- 686 • The polar plot exhibits the main contributions when air masses blow from the airfield (E to SSE)  
687 and from the main airport terminal (NE), while the polar annulus clearly shows that maximum  
688 levels for winds blowing from the airfield are reached in the central hours of the day, i.e. during  
689 the busy airport hours. No other factors show polar plots consistent with aircraft emissions.
- 690 • Some studies also report the presence of a second mode in the accumulation range for aircraft  
691 exhausts (Kinsey et al., 2010; Lobo et al., 2012; Mazaheri et al. 2013). For example, in a study  
692 conducted at the Brisbane airport (Australia), Mazaheri et al. (2009) investigated a total of 283  
693 individual aircraft plumes during landing and takeoff (LTO) cycles and reported accumulation  
694 modes between 40 and 100 nm, more pronounced in particle number size distributions during  
695 takeoffs. These findings are also consistent with Herndon et al. (2008), who studied the  
696 emissions from in-use commercial aircraft engines downwind of operational taxi- and runways at

697 Hartsfield-Jackson Atlanta airport (USA) and reported the presence of a mode at ~65 nm  
698 associated with takeoff plumes and a smaller mode at ~25 nm associated with idle. Comparing  
699 the profile of factor 3 with clustering results, it can be noted that it fits profiles for both cluster 2  
700 and 4 (aircraft and airport-related shapes). In particular, looking at the diurnal variations, factor 3  
701 seems more related with cluster 4 than with cluster 2. Although factor 3 lacks a main peak in the  
702 nucleation range, its fingerprint (Figure 7) shows the presence of a significant second mode for  
703 particles below 14 nm, which may represent the main peak in the nucleation range reported in  
704 the literature for aircraft emissions. An apparent shift towards smaller particle sizes can be  
705 attributed to evaporative shrinkage of particles before the exhaust plumes reached the sampling  
706 site (Dall'Osto et al., 2011; Harrison et al., 2016). In this context, the total number of particles  
707 attributed by our study to the aircraft exhaust emissions will be underestimated because the  
708 lower limit of detection of SMPS curtails this second peak below 14 nm.

709  
710 In addition to the main exhaust emissions from aircraft engines, there is some evidence suggesting  
711 that this factor can also be related to supplementary contributions from other on-airport sources: the  
712 high concentrations observed for winds blowing from the main terminal (ENE) suggest a  
713 supplementary contribution from the aircraft APUs. Moreover, the peaks in particle volume at 500  
714 nm and 5  $\mu\text{m}$  can be tentatively attributed to the brake dust and tyre wear during landing and to the  
715 dust resuspension due to the turbulence created by the aircraft movements, respectively. Factor 3  
716 was hence attributed to the primary emissions from the airport.

717  
718 The *fourth factor* is a minor contributor to PNC (5.9%, c.i.<sub>95</sub> 5.8-6.1), but accounts for the main  
719 percentage of the volume distribution (41%). It has two modes in the number distribution (30 and  
720 200 nm) and a main mode in the volume distribution (400 nm). Polar plot analysis does not reveal  
721 any significant directionality toward specific local sources, but shows a marked boost during wind  
722 calm hours ( $\rho_{\text{wind speed}} = -0.54$ ) and low winds from the NNE. The daily pattern is the mirror image

723 of the air temperature, and it is positively correlated with NO<sub>2</sub> (but not with NO), PM<sub>2.5</sub> and BC and  
724 negatively correlated with O<sub>3</sub>, OX and SO<sub>2</sub>. The factor 4 can be related to the cluster 3 (nighttime  
725 pollution): they match for the 30 nm peak and they show the same diurnal patterns. These results  
726 raise the following issues: (i) the higher levels reached in calm and low wind periods may suggest  
727 that the origin of the factor is local rather than external or linked to regional transport; (ii) an origin  
728 from the airport can be excluded because of the diurnal profile (very limited airport traffic recorded  
729 overnight); (iii) the directionality toward NNE, where there are no significant emission sources,  
730 may indicate that such a factor is not linked to freshly emitted pollutant. The peak intensity during  
731 the nighttime and the significant, but weak, association with NO<sub>2</sub> are highly consistent with the  
732 chemistry driving the heterogeneous reactions of N<sub>2</sub>O<sub>5</sub> and NO<sub>3</sub> on aerosol surfaces (Seinfeld and  
733 Pandis, 2006; Bertram and Thornton, 2009; Brown and Stutz, 2012). This process has been  
734 observed in many polluted areas (e.g., Fine et al., 2008; Wang et al., 2009). In particular, Dall'Osto  
735 et al. (2009) observed that most nitrate particles in London are: (i) locally produced in urban  
736 locations during nighttime; (ii) mainly present in particles smaller than 300 nm and (iii) internally  
737 mixed with sulphate, ammonium, elemental and organic carbon. Therefore, this factor clearly  
738 depicts the condensation of secondary nitrate on pre-existing particles occurring overnight and  
739 enhanced by the air temperatures below 20°C. The analysis of CCF (Figure 9) confirms this  
740 interpretation by revealing a delay of about 2 h in maximum negative correlations with ambient  
741 temperature, which is likely linked to the time needed for the heterogeneous reactions on the surface  
742 of particles. Moreover, it would be expected that nitrate-containing particles can subsequently  
743 undergo evaporation during daytime. This latter interpretation relates well to a recent study by  
744 Squizzato et al. (2013), who reported low levels of PM<sub>2.5</sub>-bound nitrate in Venice during the warm  
745 season because of the partitioning of nitrate towards the gas-phase.

746

747 Further information can be extracted by analysing this factor. The high correlation with BC ( $\rho=0.64$   
748 with maximum correlations at 0 h lags) suggests that BC particles have a key role in the formation

749 processes by acting as condensation nuclei for nitrate aerosol. BC is a primary pollutant and is  
750 therefore directly emitted from specific combustion sources: in the study area principally industries  
751 (mainly coal power plant), shipping and traffic. However, none of these primary sources are located  
752 toward the NNE. This correlation is mostly driven by the concurrent effects of the nocturnal  
753 circulation (prevalent winds blowing from the NNE) and the lower mixing layer height reached in  
754 the coldest nighttime hours (typically at 6am). In the warmest season, the mixing height over the  
755 study area may reach 1 km or more during daytime, allowing a greater dispersion of pollutants  
756 emitted at the ground, whereas it drops down to below 100 m or less during night (Pecorari et al.,  
757 2013b). Therefore it can be speculated that locally-emitted BC particles and  $\text{NO}_x$  undergo a wide  
758 dispersion within the expanded mixing layer during the daytime and move toward the mainland  
759 because of the sea breezes. Overnight, the reduction of the mixing layer height restricts BC and  
760 nitrogen oxides emissions to a layer close to ground level. In this scenario, both the reduction in air  
761 temperatures and the increased concentrations of  $\text{NO}_x$  (Figure 2b) potentially boost the formation of  
762 nitrate aerosol in the particle-phase on BC nuclei.

763  
764 The last two factors show main super-micrometre modes for the volume distribution, respectively at  
765 2-3 and 4-6  $\mu\text{m}$ . Their contributions to the total particle volume concentrations are 21.1% and  
766 12.2%, respectively, while their shares of PNC are negligible (3 and 1.5%, respectively).  
767 Apparently, both factors also show increased levels with high winds blowing from the first NE  
768 sector and diurnal cycles inverse to the air temperature. However, despite most factors showing  
769 repetitive or cyclic daily variations, *factor 5* does not present a regular diurnal pattern, but exhibits  
770 two relatively short periods with very high contributions: 18-19 and 23-24 May. This result may  
771 indicate that it is not necessarily linked with local stationary sources and not strongly affected by  
772 micro- or meso-scale weather conditions, such as breezes. Consequently, the potential origin of this  
773 factor was investigated through the concentration weighted trajectory (CWT) analysis of the back-  
774 trajectories. Details of the adopted method are provided in Hsu et al. (2003). Results reveal a



775 potential regional origin from Central Italy (Figure S18), but also increased levels when air masses  
776 move from some populated areas of Central Europe. The best interpretation for this factor is  
777 therefore the regional/transboundary pollution transport across Italy and/or Europe.

778

779 Data analysis of *factor 6* shows increased levels for strong winds blowing from the NE sector and  
780 higher levels in the colder hours of the day. Super-micrometre particles are likely emitted from non-  
781 combustion sources. The daily cycle is very similar to that of nighttime nitrate (factor 4), BC and  
782 NO<sub>2</sub>, but no correlations are significantly high with those variables. On the contrary, factor 6 clearly  
783 shows weak negative correlations with O<sub>3</sub>, OX, wind speed, solar irradiance and air temperature.  
784 Strong winds from the NNE bring air masses from agricultural fields as well as from some places in  
785 the surroundings of the airport affected by work during the sampling campaign. Consequently, the  
786 most plausible interpretation for factor 6 is the local resuspension of large dust particles, presumed  
787 to be of crustal origin. The diurnal pattern is explained by the fact that land breezes occur at  
788 nighttime, only linking source areas to the sampling site at this time of day.

789

### 790 **3.4 Potential Sources of Black Carbon**

791 Similar to PMF factor 4, BC levels peak at 6-7am (Figures 2 and 8), when ambient temperature  
792 drops to the daily minimum. The analysis of the polar plot for BC (Figure 3) does not reveal  
793 substantial increases of concentration in any direction, but a marked rise in levels during calm wind  
794 periods. An estimation of the relative contributions of local sources upon the BC levels was then  
795 made by comparing data for winds blowing from differing sectors. Six sectors were identified  
796 according to the location of the main sources of the study area: (i) the urban area of Mestre as  
797 representative of traffic-related emissions; (ii) the main industrial zone of Porto Marghera; (iii)  
798 Venice as representative of urban emissions and shipping; (iv) the Island of Murano for  
799 glassmaking emissions; (v) the VCE airfield comprising runway, taxiway and the main terminals  
800 and (vi) remaining sector. Selected sectors and polar annulus results are provided in Table 3 and

801 Figure SI3, respectively. Data were also filtered for wind speed  $>1 \text{ m s}^{-1}$  to remove wind calm  
802 periods. Results (Figure 10) show that the BC levels are higher when air masses arise from the  
803 'other direction' sector, while they are almost constant for sectors indicative of each specific local  
804 anthropogenic source. This result is quite unexpected as soot particles are known to be emitted by  
805 most combustion sources in the area, e.g., road traffic (Pant and Harrison, 2013), aircraft (Masiol  
806 and Harrison, 2014), and ships (Lack and Corbett, 2012), while emissions from wood combustion  
807 due to domestic heating and open burning are negligible in warm periods. During daytime, none of  
808 the local sources seems to have a dominant role in influencing the levels of atmospheric soot, while  
809 the nocturnal circulation (slow winds prevalently from NNE) and the lower mixing layer height (ca.  
810 100 m) at nighttime restricts soot particles to the surface layer close to the ground.

811

#### 812 4. CONCLUSIONS

813 This study was carried out at an international airport located in an area with a very complex  
814 emission scenario with the aim of detecting and apportioning the most probable sources of particles  
815 and black carbon. The main results can be summarised as follows:

- 816 • the fingerprint of aircraft emissions on the PNSD sampled in real ambient conditions reveals a  
817 main mode at approx. 80 nm and a second mode in the nucleation range below the lower limit  
818 for particle detection of the SMPS ( $<14 \text{ nm}$ ). Air traffic contributes about 22% of PNC, but does  
819 not contribute significantly to the mass concentrations of black carbon. However, the size  
820 distribution fingerprint could be affected by evaporative processes which have shifted the  
821 particle size below 14 nm and, thus, the total amount of particles emitted by the airport could be  
822 underestimated;
- 823 • nucleation particles with a mode at 15-20 nm are the main contributors to PNC (44%) and may  
824 be linked to both photochemical nucleation from precursor gases and the evolution of primary  
825 particles emitted by several combustion processes and undergoing  
826 condensation/evaporation/dilution processes after emission. Cluster analysis has helped to

827 identify and quantify the midday nucleation episodes, which were recorded for about 40% of  
828 sampling days;

- 829 • the emissions of road traffic from the main urban area and shipping traffic around the city of  
830 Venice contributes to ~26% of PNC (mode at 35-40 nm);
- 831 • Coarse particles originated from nighttime nitrate formation and from resuspension advected by  
832 regional transport are the main contributors to the particle volume concentrations and, therefore,  
833 mass concentrations, as clearly indicated by significant positive correlations with  $PM_{2.5}$ ;
- 834 • levels of black carbon are strongly associated with the dynamics of the mixing layer, while no  
835 specific local sources can be identified as dominant in the study area. BC also has an important  
836 role by providing condensation nuclei for nighttime secondary nitrate aerosol formation.

837

838 In summary, sources related to transport sectors are amongst the largest contributors to local air  
839 pollutant concentrations. Beside aircraft traffic, airports are often located near major cities and  
840 attract large volumes of road traffic, which are additive to the local pollution. Furthermore, micro-  
841 and meso-scale meteorology may move, mix and transform emitted primary pollutants. It is  
842 therefore very difficult to differentiate between pollutants arising from airport operations and those  
843 from other local sources. The approaches proposed in this study have successfully identified and  
844 apportioned the main potential sources in an area affected by a complex emission scenario and the  
845 results can be utilised to plan local air pollution control measures.

846

847 This study is the first to apply cluster analysis and receptor modelling techniques for assessing the  
848 sources of wide-range particle size spectra at an international airport. Although such techniques are  
849 widely used to detect and quantify the sources of airborne particles (both for mass and number  
850 concentrations), their application to data collected near airports, or even inside the airfields, is still  
851 very limited. There are a number of reasons for this as studies at airports must face several issues:  
852 (i) the need of specific authorisations to enter the airport area for carrying chemical substances

853 and/or radioactive sources required by some scientific equipment; (ii) the space and time allowed  
854 for research is strictly limited for compliance with the strong security standards of airports; (iii) the  
855 positioning of sampling sites is also restricted to fulfil security standards. For these reasons,  
856 limitations affected this study, such as the length of the sampling campaign and the location of the  
857 sampling site. They both represent the best compromise between stringent safety measures for  
858 flights and scientific investigation.

859

## 860 **ACKNOWLEDGEMENTS**

861 The authors gratefully acknowledge: (i) the European Union for funding the Marie Curie Intra-  
862 European Fellowship for career development to M. Masiol through the project entitled 'Chemical  
863 and Physical Properties and Source Apportionment of Airport Emissions in the context of European  
864 Air Quality Directives (Project CHEERS, call: FP7-PEOPLE-2012-IEF, proposal no. 328542); (ii)  
865 SAVE S.p.A. (Davide Bassano, Saverio Sollecito) for logistic, technical support and for supplying  
866 aircraft movement data; (iii) Ente Zona Industriale di Porto Marghera ([www.entezona.it](http://www.entezona.it)) for  
867 providing some pollutant and weather data; (iv) Stefania Squizzato (Ca' Foscari University of  
868 Venice) and Gianni Formenton (ARPAV) for the valuable exchange of information and discussion.  
869 The authors gratefully acknowledge the NOAA Air Resources Laboratory (ARL) for the provision  
870 of the HYSPLIT transport and dispersion model used in this publication.

871

872

## REFERENCES

- 874 Anderson, B.E., Branham, H.-S., Hudgins, C.H., Plant, J.V., Ballenthin, J.O., Miller, T.M.,  
875 Viggiano, A.A., Blake, D.R., Boudries, H., Canagaratna, M., Miake-Lye, R.C., Onasch, T.,  
876 Wormhoudt, J., Worsnop, D., Brunke, K.E., Culler, S., Penko P., Sanders, T., Han, H.-S., Lee, P.,  
877 Pui, D.Y.H., Thornhill, K.L., Winstead, E.L., 2005. Experiment to Characterize Aircraft Volatile  
878 Aerosol and Trace-Species Emissions (EXCAVATE). NASA/TM-2005-213783. National  
879 Aeronautics and Space Administration, Hampton, VA. August 2005.
- 880  
881 ARPAV, 2014. INEMAR Veneto, Inventario emissioni in atmosfera: emissioni in Regione Veneto,  
882 edizione 2007/8 - dati definitivi. ARPA Veneto and Regione Veneto. Available from:  
883 <http://89.96.234.242/inemar/webdata/main.seam> (last accessed on January 2014).
- 884  
885 ARPAV – Regione Veneto, 2015. INEMAR VENETO 2010 - Inventario Regionale delle Emissioni  
886 in Atmosfera in Regione Veneto, edizione 2010 – dati in versione definitiva. ARPA Veneto -  
887 Osservatorio Regionale Aria, Regione del Veneto - Dipartimento Ambiente, Sezione Tutela  
888 Ambiente, Settore Tutela Atmosfera.
- 889  
890 Beddows, D.C.S., Dall'Osto, M., Harrison, R.M., 2009. Cluster analysis of rural, urban and  
891 curbside atmospheric particle size data. *Environ. Sci. Technol.* 43, 4694–4700.
- 892  
893 Beddows, D.C.S., Dall'Osto, M., Harrison, R.M., 2010. An enhanced procedure for the merging of  
894 atmospheric particle size distribution data measured using electrical mobility and time-of-flight  
895 analysers. *Aerosol Sci. Technol.* 44, 930–938.
- 896  
897 Beddows, D.C.S., Dall'Osto, M., Harrison, R. M., Kulmala, M., Asmi, A., Wiedensohler, A., Laj,  
898 P., Fjaeraa, A.M., Sellegri, K., Birmili, W., Bukowiecki, N., Weingartner, E., Baltensperger, U.,  
899 Zdimal, V., Zikova, N., Putaud, J.-P., Marinoni, A., Tunved, P., Hansson, H.-C., Fiebig, M.,  
900 Kivekäs, N., Swietlicki, E., Lihavainen, H., Asmi, E., Ulevicius, V., Aalto, P. P., Mihalopoulos, N.,  
901 Kalivitis, N., Kalapov, I., Kiss, G., de Leeuw, G., Henzing, B., O'Dowd, C., Jennings, S. G., Flentje,  
902 H., Meinhardt, F., Ries, L., Denier van der Gon, H. A. C., Visschedijk, A. J. H., 2014. Variations in  
903 tropospheric submicron particle size distributions across the European continent 2008–2009.  
904 *Atmos. Chem. Phys.* 14, 4327–4348.
- 905  
906 Beelen, R., Raaschou-Nielsen, O., Stafoggia, M., Andersen, Z.J., Weinmayr, G., Hoffmann, B.,  
907 Wolf K., Samoli, E., Fischer, P., Nieuwenhuijsen, M., Vineis, P., Xun, W.W., Katsouyanni, K.,  
908 Dimakopoulou, K., Oudin, A., Forsberg, B., Modig, L., Havulinna, A.S., Lanki, T., Turunen, A.,  
909 Oftedal, B., Nystad, W., Nafstad, P., De Faire, U., Pedersen, N.L., Östenson, C.G., Fratiglioni, L.,  
910 Penell, J., Korek, M., Pershagen, G., Thorup Eriksen, K., Overvad, K., Ellermann, T., Eeftens, M.,  
911 Peeters, P.H., Meliefste, K., Wang, M., Bueno-de-Mesquita, B., Sugiri, D., Krämer, U., Geinrich, J.,  
912 de Hoogh, K., Key, T., Peters, A., Hampel, R., Concin, H., Nagel, G., Ineichen, A., Schaffner, E.,  
913 Probst-Hensch, N., Künzli, N., Schindler, C., Schikowski, T., Adam, M., Phuleria, H., Vilier, A.,  
914 Clavel-Chapelon, F., Declercq, C., Grioni, S., Krogh, V., Tsai, M.-Y., Ricceri, F., Sacerdote, C.,  
915 Galassi, C., Migliore, E., Ranzi, A., Cesaroni, G., Badaloni, C., Forastiere, F., Tamayo, I., Amiano,  
916 P., Dorronsoro, M., Katsoulis, M., Trichopoulou, A., Brunekreef, B., Hoek, G., 2014. Effects of  
917 long-term exposure to air pollution on natural-cause mortality: an analysis of 22 European cohorts  
918 within the multicentre ESCAPE project. *Lancet* 383, 785–795.
- 919  
920 Belis, C.A., Larsen, B.R., Amato, F., El Haddad, I., Favez, O., Harrison, R.M., Hopke, P.K., Nava,  
921 S., Paatero, P., Prévôt, A., Quass, U., Vecchi, R., Viana, M., 2014. European guide on air pollution  
922 source apportionment with receptor models. JRC Reference Reports EUR26080 EN
- 923

- 924 Bertram, T. H., Thornton, J. A., 2009. Toward a general parameterization of N<sub>2</sub>O<sub>5</sub> reactivity on  
925 aqueous particles: the competing effects of particle liquid water, nitrate and chloride. *Atmos. Chem.*  
926 *Phys.* 9, 8351-8363.
- 927
- 928 Brines, M., Dall'Osto, M., Beddows, D.C.S., Harrison, R. M., Querol, X., 2014. Simplifying aerosol  
929 size distributions modes simultaneously detected at four monitoring sites during SAPUSS. *Atmos.*  
930 *Chem. Phys.* 14, 2973-2986.
- 931
- 932 Brines, M., Dall'Osto, M., Beddows, D., Harrison, R., Gómez-Moreno, F., Núñez, L., Artíñano, B.,  
933 Costabile, F., Gobbi, G., Salimi, F., 2015. Traffic and nucleation events as main sources of ultrafine  
934 particles in high-insolation developed world cities. *Atmos. Chem. Phys.* 15, 5929-5945.
- 935
- 936 Brown, S.S., Stutz, J., 2012. Nighttime radical observations and chemistry. *Chem. Soc. Rev.* 41,  
937 6405–6447.
- 938
- 939 Brown, S.G., Eberly, S., Paatero, P., Norris, G.A., 2015. Methods for estimating uncertainty in  
940 PMF solutions: Examples with ambient air and water quality data and guidance on reporting PMF  
941 results. *Sci.Total Environ.* 518, 626-635.
- 942
- 943 Carslaw, D.C., Ropkins, K., 2012. openair - an R package for air quality data analysis. *Environ.*  
944 *Model. Softw.* 27-28, 52-61.
- 945
- 946 Carslaw, D.C., Beevers, S.D., Ropkins, K., Bell, M.C., 2006. Detecting and quantifying aircraft and  
947 other on-airport contributions to ambient nitrogen oxides in the vicinity of a large international  
948 airport. *Atmos. Environ.* 40, 5424–5434.
- 949
- 950 Carslaw, D.C., Beevers, S.D., Bell, M.C., 2007. Risks of exceeding the hourly EU limit value for  
951 nitrogen dioxide resulting from increased road transport emissions of primary nitrogen dioxide.  
952 *Atmos. Environ.* 41, 2073-2082.
- 953
- 954 Charron, A., Harrison, R.M., 2003. Primary particle formation from vehicle emissions during  
955 exhaust dilution in the roadside atmosphere. *Atmos. Environ.* 37, 4109–4119.
- 956
- 957 Chen, J.P., Tsai, T.S., Liu, S.C., 2011. Aerosol nucleation spikes in the planetary boundary layer.  
958 *Atmos. Chem. Phys.* 11, 7171-7184.
- 959
- 960 Cheung, H. C., Morawska, L., Ristovski, Z. D., and Wainwright, D., 2012. Influence of medium  
961 range transport of particles from nucleation burst on particle number concentration within the urban  
962 airshed. *Atmos. Chem. Phys.* 12, 4951-4962.
- 963
- 964 Costabile, F., Birmili, W., Klose, S., Tuch, T., Wehner, B., Wiedensohler, A., Franck, U., König,  
965 K., Sonntag, A., 2009. Spatio-temporal variability and principal components of the particle number  
966 size distribution in an urban atmosphere. *Atmos. Chem. Phys.* 9, 3163-3195.
- 967
- 968 Contini, D., Gambaro, A., Donato, A., Cescon, P., Cesari, D., Merico, E., Citron, M., 2015. Inter-  
969 annual trend of the primary contribution of ship emissions to PM 2.5 concentrations in Venice  
970 (Italy): Efficiency of emissions mitigation strategies. *Atmos. Environ.* 102, 183-190.
- 971
- 972 Cyrus, J., Eeftens, M., Heinrich, J., Ampe, C., Armengaud, A., Beelen, R., Bellander, T.,  
973 Beregszaszi, T., Birk, M., Cesaroni, G., Cirach, M., de Hoogh, K., De Nazelle, A., de Vocht, F.,  
974 Declercq C., Dedele, A., Dimakopoulou, K., Eriksen, K., Galassi, C., Grauleviciene, R., Grivas, G.,  
975 Gruzjeva, O., Hagenbjörk Gustafsson, A., Hoffmann, B., Iakovides, M., Ineichen, A., Krämer, U.,

- 976 Lanki, T., Lozano, P., Madsen, C., Meliefste, K., Modig, L., Mølterm, A., Mosler, G.,  
977 Nieuwenhuijsen, M., Nonnemacher, M., Oldenwening, M., Peters, A., Pontet, S., Probst-Hensch,  
978 N., Quass, U., Raaschou-Nielsen, O., Ranzi, A., Sugiri, D., Stephanou, E.G., Taimisto, P., Tsai, M.-  
979 Y., Vaskövi, E., Villani, S., Wang, M., Brunekreef, B., Hoek, G., 2012. Variation of NO<sub>2</sub> and NO<sub>x</sub>  
980 concentrations between and within 36 European study areas: Results from the ESCAPE study.  
981 *Atmos. Environ.* 62, 374–390.  
982
- 983 Dal Maso, M., Kulmala, M., Riipinen, I., Wagner, R., Hussein, T., Aalto, P.P. Lehtinen, K.E., 2005.  
984 Formation and growth of fresh atmospheric aerosols: eight years of aerosol size distribution data  
985 from SMEAR II, Hyytiälä, Finland. *Boreal Env. Res.* 10(5), p.323.  
986
- 987 Dall'Osto, M., Harrison, R.M., Coe, H., Williams, P.I., Allan, J.D., 2009. Real time chemical  
988 characterization of local and regional nitrate aerosols. *Atmos. Chem. Phys.* 9, 3709-3720.  
989
- 990 Dall'Osto, M., Thorpe, A., Beddows, D.C.S., Harrison, R.M., Barlow, J.F., Dunbar, T., Williams,  
991 P.I., Coe, H., 2011. Remarkable dynamics of nanoparticles in the urban atmosphere. *Atmos. Chem.*  
992 *Phys.* 11, 6623-6637.  
993
- 994 Dall'Osto, M., Beddows, D.C.S., Pey, J., Rodriguez, S., Alastuey, A., Harrison, Roy M., Querol, X.,  
995 2012. Urban aerosol size distributions over the Mediterranean city of Barcelona, NE Spain. *Atmos.*  
996 *Chem. Phys.* 12, 10693-10707.  
997
- 998 Dall'Osto, M., Querol, X., Alastuey, A., O'Dowd, C., Harrison, R.M., Wenger, J. and Gómez,  
999 Moreno, F.J., 2013. On the spatial distribution and evolution of ultrafine particles in Barcelona.  
1000 *Atmos. Chem. Phys.* 13, 741-759.  
1001
- 1002 Dodson, R.E., Houseman, E.A., Morin, B., Levy, J.I., 2009. An analysis of continuous black carbon  
1003 concentrations in proximity to an airport and major roadways. *Atmos. Environ.* 43, 3764-3773.  
1004
- 1005 Fine, P.M., Sioutas, C., Solomon, P.A., 2008. Secondary particulate matter in the United States:  
1006 Insights from the Particulate Matter Supersites Program and related studies. *JAWMA* 58, 234–253.  
1007
- 1008 Fiore, A.M., Naik, V., Spracklen, D.V., Steiner, A., Unger, N., Prather, M., Bergmann, D.,  
1009 Cameron-Smith, P.J., Cionni, I., Collins, W.J., Dalsøren, S., Eyring, V., Folberth, G.A., Ginoux, P.,  
1010 Horowitz, L.W., Josse, B., Lamarque, J.-F., MacKenzie, I.A., Nagashima, T., O'Connor, F.M.,  
1011 Righi, M., Rumbold, S.T., Shindell, D.T., Skeie, R.B., Sudo, K., Szopa, S., Takemura, T., Zeng, G.,  
1012 2012. Global air quality and climate. *Chem. Soc. Rev.* 41, 6663-6683.  
1013
- 1014 Friend, A.J., Ayoko, G.A., Jager, D., Wust, M., Jayaratne, E.R., Jamriska, M. Morawska, L., 2013.  
1015 Sources of ultrafine particles and chemical species along a traffic corridor: comparison of the results  
1016 from two receptor models. *Environ. Chem.* 10(1), 54-63.  
1017
- 1018 González, Y., Rodríguez, S., 2013. A comparative study on the ultrafine particle episodes induced  
1019 by vehicle exhaust: A crude oil refinery and ship emissions. *Atmos. Res.* 120, 43-54.  
1020
- 1021 Grice, S., Stedman, J., Kent, A., Hobson, M., Norris, J., Abbott, J., Cooke S., 2009. Recent trends  
1022 and projections of primary NO<sub>2</sub> emissions in Europe. *Atmos. Environ.* 43, 2154-2167.  
1023
- 1024 Hamed, A., Joutsensaari, J., Mikkonen, S., Sogacheva, L., Dal Maso, M., Kulmala, M., Cavalli, F.,  
1025 Fuzzi, S., Facchini, M. C., Decesari, S., Mircea, M., Lehtinen, K. E. J., Laaksonen, A., 2007.  
1026 Nucleation and growth of new particles in Po Valley, Italy. *Atmos. Chem. Phys.* 7, 355-376.  
1027

- 1028 Harrison, R.M., Jones, A.M., Beddows, D.C.S., Dall'Osto, M., Nikolova, I., 2016. Evaporation of  
1029 traffic-generated nanoparticles during advection from source. *Atmos. Environ.* 125, 1-7.  
1030
- 1031 Harrison, R.M., Beddows, D.C.S., Dall'Osto, M., 2011. PMF Analysis of wide-range particle size  
1032 spectra collected on a major highway. *Environ. Sci. Technol.* 45, 5522–5528.  
1033 Heal, M. R., Kumar, P., Harrison, R. M., 2012. Particles, air quality, policy and health. *Chem. Soc.*  
1034 *Rev.* 41, 6606-6630.  
1035
- 1036 Healy, R.M., O'Connor, I.P., Hellebust, S., Allanic, A., Sodeau, J.R., Wenger, J.C., 2009.  
1037 Characterisation of single particles from in-port ship emissions. *Atmos. Environ.* 43, 6408-6414.  
1038 Herndon, S.C., Jayne, J.T., Lobo, P., Onasch, T.B., Fleming, G., Hagen, D.E., Whitefield, P.D.,  
1039 Miake-Lye, R.C., 2008. Commercial aircraft engine emissions characterization of in-use aircraft at  
1040 Hartsfield-Jackson Atlanta International Airport. *Environ. Sci. Technol.* 42, 1877-1883.  
1041 Hirsikko, A., Vakkari, V., Tiitta, P., Hatakka, J., Kerminen, V.-M., Sundström, A.-M., Beukes, J.  
1042 P., Manninen, H.E., Kulmala, M., Laakso, L., 2013. Multiple daytime nucleation events in semi-  
1043 clean savannah and industrial environments in South Africa: analysis based on observations. *Atmos.*  
1044 *Chem. Phys.* 13, 5523-5532.  
1045
- 1046 Hopke, P.K., 2016. Review of receptor modeling methods for source apportionment. *J. Air Waste*  
1047 *Manage. Assoc.* doi:10.1080/10962247.2016.1140693.  
1048
- 1049 Hsu, Y.K., Holsen, T.M., Hopke, P.K., 2003. Comparison of hybrid receptor models to locate PCB  
1050 sources in Chicago. *Atmos. Environ.* 37, 545-562.  
1051
- 1052 Hudda, N, Gould, T., Hartin, K., Larson, T.V., Fruin, S.A., 2014. Emissions from an international  
1053 airport increase particle number concentrations 4-fold at 10 km downwind. *Environ. Sci. Technol.*  
1054 48, 6628–6635.  
1055
- 1056 Hussein, T., Molgaard, B., Hannuniemi, H., Martikainen, J., Järvi, L., Wegner, T., Ripamonti,  
1057 G., Weber, S., Vesala, T., Hämeri, K., 2014. Fingerprints of the urban particle number size  
1058 distribution in Helsinki, Finland: Local vs. regional characteristics. *Boreal Env. Res.* 19, 1–20.  
1059
- 1060 ICAO, 2008. Environmental Protection (Annex 16), Vol. 2 – Aircraft Engine Emission,  
1061 International Civil Aviation Organization, International Standards and Recommended Practices,  
1062 ISBN 978-92-9231-123-0.  
1063
- 1064 Janhäll S., Jonsson Å.M., Molnár P., Svensson E.A., Hallquist M., 2004. Size resolved traffic  
1065 emission factors of submicrometer particles. *Atmos. Environ.* 38, 4331–4340.  
1066
- 1067 Janssen, R.H.H., Vilà-Guerau de Arellano, J., Ganzeveld, L.N., Kabat, P., Jimenez, J.L., Farmer,  
1068 D.K., van Heerwaarden, C.C., Mammarella, I., 2012. Combined effects of surface conditions.  
1069 boundary layer dynamics and chemistry on diurnal SOA evolution. *Atmos. Chem. Phys.* 12, 6827-  
1070 6843.  
1071
- 1072 Jonsson, Å.M., Westerlund, J., Hallquist, M., 2011. Size-resolved particle emission factors for  
1073 individual ships. *Geophys. Res. Lett.* 38, L13809.  
1074
- 1075 Kasper, A., Aufdenblatten, S., Forss, A., Mohr, M., Burtscher, H., 2007. Particulate emissions from  
1076 a low-speed marine diesel engine. *Aerosol Sci. Technol.* 41, 24-32.  
1077



- 1078 Keuken, M.P., Moerman, M., Zandveld, P., Henzing, J.S., Hoek, G., 2015. Total and size-resolved  
1079 particle number and black carbon concentrations in urban areas near Schiphol airport (the  
1080 Netherlands). *Atmos. Environ.* 104 132-142.
- 1081
- 1082 Kinsey, J.S., Dong, Y., Williams, D.C., Logan, R., 2010. Physical characterization of the fine  
1083 particle emissions from commercial aircraft engines during the aircraft particle emissions  
1084 experiment (APEX) 1 to 3. *Atmos. Environ.* 44, 2147-2156.
- 1085
- 1086 Kivekäs, N., Massling, A., Grythe, H., Lange, R., Rusnak, V., Carreno, S., Skov, H., Swietlicki, E.,  
1087 Nguyen, Q. T., Glasius, M., Kristensson, A., 2014. Contribution of ship traffic to aerosol particle  
1088 concentrations downwind of a major shipping lane. *Atmos. Chem. Phys.* 14, 8255-8267.
- 1089
- 1090 Kley, D., Kleinmann, M., Sanderman, H., Krupa, S., 1999. Photochemical oxidants: state of the  
1091 science. *Environ. Pollut.* 100, 19-42.
- 1092
- 1093 Kulmala, M. Kerminen, V.-M., 2008. On the formation and growth of atmospheric nanoparticles.  
1094 *Atmos. Res.* 90, 132–150.
- 1095
- 1096 Kulmala, M., Asmi, A., Lappalainen, H. K., Baltensperger, U., Brenguier, J.-L., Facchini, M. C.,  
1097 Hansson, H.-C., Hov, Ø., O'Dowd, C. D., Pöschl, U., Wiedensohler, A., Boers, R., Boucher, O., de  
1098 Leeuw, G., Denier van der Gon, H. A. C., Feichter, J., Krejci, R., Laj, P., Lihavainen, H., Lohmann,  
1099 U., McFiggans, G., Mentel, T., Pilinis, C., Riipinen, I., Schulz, M., Stohl, A., Swietlicki, E.,  
1100 Vignati, E., Alves, C., Amann, M., Ammann, M., Arabas, S., Artaxo, P., Baars, H., Beddows, D. C.  
1101 S., Bergström, R., Beukes, J. P., Bilde, M., Burkhardt, J. F., Canonaco, F., Clegg, S. L., Coe, H.,  
1102 Crumeyrolle, S., D'Anna, B., Decesari, S., Gilardoni, S., Fischer, M., Fjaeraa, A. M., Fountoukis,  
1103 C., George, C., Gomes, L., Halloran, P., Hamburger, T., Harrison, R. M., Herrmann, H., Hoffmann,  
1104 T., Hoose, C., Hu, M., Hyvärinen, A., Hörrak, U., Iinuma, Y., Iversen, T., Josipovic, M.,  
1105 Kanakidou, M., Kiendler-Scharr, A., Kirkevåg, A., Kiss, G., Klimont, Z., Kolmonen, P., Komppula,  
1106 M., Kristjánsson, J.-E., Laakso, L., Laaksonen, A., Labonnote, L., Lanz, V. A., Lehtinen, K. E. J.,  
1107 Rizzo, L. V., Makkonen, R., Manninen, H. E., McMeeking, G., Merikanto, J., Minikin, A., Mirme,  
1108 S., Morgan, W. T., Nemitz, E., O'Donnell, D., Panwar, T. S., Pawlowska, H., Petzold, A., Pienaar,  
1109 J. J., Pio, C., Plass-Duelmer, C., Prévôt, A. S. H., Pryor, S., Reddington, C. L., Roberts, G.,  
1110 Rosenfeld, D., Schwarz, J., Seland, Ø., Sellegri, K., Shen, X. J., Shiraiwa, M., Siebert, H., Sierau,  
1111 B., Simpson, D., Sun, J. Y., Topping, D., Tunved, P., Vaattovaara, P., Vakkari, V., Veefkind, J. P.,  
1112 Visschedijk, A., Vuollekoski, H., Vuolo, R., Wehner, B., Wildt, J., Woodward, S., Worsnop, D. R.,  
1113 van Zadelhoff, G.-J., Zardini, A. A., Zhang, K., van Zyl, P. G., Kerminen, V.-M., S Carslaw, K.,  
1114 and Pandis, S. N., 2011. General overview: European Integrated project on Aerosol Cloud Climate  
1115 and Air Quality interactions (EUCAARI) – integrating aerosol research from nano to global scales.  
1116 *Atmos. Chem. Phys.* 11, 13061-13143.
- 1117
- 1118 Lack, D.A., Corbett, J.J., 2012. Black carbon from ships: a review of the effects of ship speed, fuel  
1119 quality and exhaust gas scrubbing. *Atmos. Chem. Phys.* 12, 3985–4000.
- 1120
- 1121 Lee, D.S., Fahey, D.W., Forster, P.M., Newton, P.J., Wit, R.C.N., Lim, L.L., Owen, B., Sausen, R.,  
1122 2009. Aviation and global climate change in the 21st century. *Atmos. Environ.* 43, 3520-3537.
- 1123
- 1124 Liu, X., Wang, W., Liu, H., Geng, C., Zhang, W., Wang, H., Liu, Z., 2010. Number size  
1125 distribution of particles emitted from two kinds of typical boilers in a coal-fired power plant in  
1126 China. *Energy Fuels* 24(3), 1677-1681.
- 1127

- 1128 Lobo, P., Hagen, D.E., Whitefield, P.D., 2012. Measurement and analysis of aircraft engine PM  
1129 emissions downwind of an active runway at the Oakland International Airport. *Atmos. Environ.* 61,  
1130 114-123.
- 1131
- 1132 Lobo, P., Hagen, D. E., Whitefield, P. D., Raper, D., 2015. PM emissions measurements of in-  
1133 service commercial aircraft engines during the Delta-Atlanta Hartsfield Study. *Atmos. Environ.*  
1134 104, 237-245.
- 1135
- 1136 Lyyräinen, J., Jokiniemi, J., Kauppinen, E.I., Joutsensaari, J., 1999. Aerosol characterisation in  
1137 medium-speed diesel engines operating with heavy fuel oils. *J. Aerosol Sci.* 30, 771-784.
- 1138
- 1139 Masiol, M., Harrison, R.M., 2014. Aircraft engine exhaust emissions and other airport-related  
1140 contributions to ambient air pollution: A review. *Atmos. Environ.* 95, 409-455.
- 1141
- 1142 Masiol, M., Squizzato, S., Rampazzo, G., Pavoni, B., 2014a. Source apportionment of PM<sub>2.5</sub> at  
1143 multiple sites in Venice (Italy): Spatial variability and the role of weather. *Atmos. Environ.* 98, 78-  
1144 88.
- 1145
- 1146 Masiol, M., Agostinelli, C., Formenton, G., Tarabotti, E., Pavoni, B., 2014b. Thirteen years of air  
1147 pollution hourly monitoring in a large city: Potential sources, trends, cycles and effects of car-free  
1148 days. *Sci. Total Environ.* 494-495, 84-96.
- 1149
- 1150 Mazaheri, M., Johnson, G.R., Morawska, L., 2009. Particle and gaseous emissions from  
1151 commercial aircraft at each stage of the landing and takeoff cycle. *Environ. Sci. Technol.* 43, 441-  
1152 446.
- 1153
- 1154 Mazaheri, M., Bostrom, T.E., Johnson, G.R., Morawska, L., 2013. Composition and morphology of  
1155 particle emissions from in-use aircraft during takeoff and landing. *Environ. Sci. Technol.* 47, 5235-  
1156 5242.
- 1157
- 1158 Modini, R.L., Ristovski, Z.D., Johnson, G.R., He, C., Surawski, N., Morawska, L., Suni, T.,  
1159 Kulmala, M., 2009. New particle formation and growth at a remote, sub-tropical coastal location.  
1160 *Atmos. Chem. Phys.* 9, 7607-7621.
- 1161
- 1162 Nielsen, M. T., Livbjerg, H., Fogh, C. L., Jensen, J. N., Simonsen, P., Lund, C., Poulsen, K.,  
1163 Sander, B., 2002. Formation and emission of fine particles from two coal-fired power plants. *Comb.*  
1164 *Sci. Technol.* 174(2), 79-113.
- 1165
- 1166 Ntziachristos, L., Ning, Z. Geller, M.D., Sioutas, C., 2007. Particle concentration and characteristics  
1167 near a major freeway with heavy-duty diesel traffic. *Environ. Sci. Technol.* 41, 2223-2230.
- 1168
- 1169 O'Dowd, C.D., Hoffmann, T., 2006. Coastal new particle formation: A review of the current state-  
1170 of-the-art. *Environ. Chem.* 2, 245-255.
- 1171
- 1172 O'Dowd, C.D., De Leeuw, G., 2007. Marine aerosol production: A review of the current  
1173 knowledge. *Philos. Roy. Soc. A.* 365, 1753-1774.
- 1174
- 1175 O'Dowd, C., McFiggans, G., Creasey, D. J., Pirjola, L., Hoell, C., Smith, M.H., Allan, B.J., Plane,  
1176 J.M.C., Heard, D.E., Lee, J.D., Pilling, M.J., Kulmala, M., 1999. On the photochemical production  
1177 of new particles in the coastal boundary layer. *Geophys. Res. Lett.* 26, 1707-1710.
- 1178

- 1179 Ogulei, D., Hopke, P.K., Wallace, L.A., 2006. Analysis of indoor particle size distributions in an  
1180 occupied townhouse using positive matrix factorization. *Indoor Air* 16(3), 204-215.  
1181
- 1182 Ogulei, D. , Hopke, P.K. , Chalupa, D.C., Utell, M.J., 2007. Modeling source contributions to  
1183 submicron particle number concentrations measured in Rochester, New York. *Aerosol Sci. Technol.*  
1184 41, 179-201.  
1185
- 1186 Paatero, P., 1997. Least squares formulation of robust non-negative factor analysis. *Chemom. Intell.*  
1187 *Lab. Syst.* 37, 23-35.  
1188
- 1189 Paatero, P., Tapper, U., 1994. Positive matrix factorization: a non-negative factor model with  
1190 optimal utilization of error estimates of data values. *Environmetrics* 5, 111-126.  
1191
- 1192 Paatero, P., Hopke, P.K., Song, X H., Ramadan, Z., 2002. Understanding and controlling rotations  
1193 in factor analytic models. *Chemom. Intell. Lab. Syst.* 60, 253–264.  
1194
- 1195 Paatero, P., Eberly, S., Brown, S.G., Norris, G.A., 2014. Methods for estimating uncertainty in  
1196 factor analytic solutions. *Atmos. Meas. Tech.* 7, 781-797.  
1197
- 1198 Pant, P., Harrison, R.M., 2013. Estimation of the contribution of road traffic emissions to  
1199 particulate matter concentrations from field measurements: a review. *Atmos. Environ.* 77, 78-97.  
1200
- 1201 Pecorari, E., Squizzato, S., Ferrari, A., Cuzzolin, G., Rampazzo G., 2013a. WATERBUS: A model  
1202 to estimate boats' emissions in "water cities". *Transport. Res. D-TR E*, 23, 73-80.  
1203
- 1204 Pecorari, E., Squizzato, S., Masiol, M., Radice, P., Pavoni, B., Rampazzo, G., 2013b. Using a  
1205 photochemical model to assess the horizontal, vertical and time distribution of PM<sub>2.5</sub> in a complex  
1206 area: Relationships between the regional and local sources and the meteorological conditions. *Sci.*  
1207 *Total Environ.* 443, 681–691.  
1208
- 1209 Pecorari, E., Mantovani, A., Franceschini, C., Bassano, D., Palmeri, L., Grancazzo, G., 2015.  
1210 Analysis of the effects of meteorology on aircraft exhaust dispersion and deposition using a  
1211 Lagrangian particle model. *Sci Total Environ.* 541, 839–856.  
1212
- 1213 Petzold, A., Weingartner, E., Hasselbach, J., Lauer, P., Kurok, C., Fleischer, F., 2010. Physical  
1214 properties, chemical composition, and cloud forming potential of particulate emissions from a  
1215 marine diesel engine at various load conditions. *Environ. Sci. Technol.* 44, 3800-3805.  
1216
- 1217 R Core Team, 2015. R: A language and environment for statistical computing. R Foundation for  
1218 Statistical Computing, Vienna, Austria. URL <http://www.R-project.org/>.  
1219
- 1220 Reche, C., Querol, X., Alastuey, A., Viana, M., Pey, J., Moreno, T., Rodriguez, S., Gonzalez, Y.,  
1221 Fernandez-Camacho, R., Sanchez de la Campa, A.M., de la Rosa, J., Dall'Osto, M., Prevot, A.S.H.,  
1222 Hueglin, C., Harrison, R.M. and Quincey, P., 2011. New considerations for pm, black carbon and  
1223 particle number concentration for air quality monitoring across different European cities. *Atmos.*  
1224 *Chem. Phys.* 11, 6207-6227.  
1225
- 1226 Reff, A., Eberly, S.I., Bhave, P.V., 2007. Receptor modeling of ambient particulate matter data  
1227 using positive matrix factorization: review of existing methods. *JAWMA* 57, 146-154.  
1228

- 1229 Rodríguez, S., Van Dingenen, R., Putaud, J.P., Martins-Dos Santos, S. Roselli, D., 2005. Nucleation  
1230 and growth of new particles in the rural atmosphere of Northern Italy—relationship to air quality  
1231 monitoring. *Atmos. Environ.* 39(36), 6734-6746.  
1232
- 1233 Salimi, F., Ristovski, Z., Mazaheri, M., Laiman, R., Crilley, L.R., He, C., Clifford, S., Morawska,  
1234 L., 2014. Assessment and application of clustering techniques to atmospheric particle number size  
1235 distribution for the purpose of source apportionment. *Atmos. Chem. Phys.* 14, 11883-11892.  
1236
- 1237 Seinfeld, J.H., Pandis, S.N., 2006. *Atmospheric Chemistry and Physics*, second ed.. In: *From Air*  
1238 *Pollution to Climate Change* John Wiley & Sons, NewYork.  
1239
- 1240 Shi, J.P., Harrison, R.M., 1999. Investigation of ultrafine particle formation during diesel exhaust  
1241 dilution. *Environ. Sci. Technol.* 33, 3730-3736.  
1242
- 1243 Squizzato, S., Masiol, M., Brunelli, A., Pistollato, S., Tarabotti, E., Rampazzo, G., Pavoni, B.,  
1244 2013. Factors determining the formation of secondary inorganic aerosol: a case study in the Po  
1245 Valley (Italy). *Atmos. Chem. Phys.* 13, 1927-1939.  
1246
- 1247 Squizzato, S., Masiol, M., 2015. Application of meteorology-based methods to determine local and  
1248 external contributions to particulate matter pollution: A case study in Venice (Italy). *Atmos.*  
1249 *Environ.* 119, 69-81.  
1250
- 1251 Stanier, C. O., Khlystov, A. Y. and Pandis, S. N., 2004. Nucleation Events During the Pittsburgh  
1252 Air Quality Study: Description and Relation to Key Meteorological, Gas Phase, and Aerosol  
1253 Parameters. *Aerosol Sci. Technol.* 38, 253–264.  
1254
- 1255 Stevens, R. G., Pierce, J. R., Brock, C. A., Reed, M. K., Crawford, J. H., Holloway, J. S., Ryerson,  
1256 T. B., Huey, L. G., Nowak, J. B., 2012. Nucleation and growth of sulfate aerosol in coal-fired  
1257 power plant plumes: sensitivity to background aerosol and meteorology. *Atmos. Chem. Phys.*, 12,  
1258 189-206.  
1259
- 1260 USEPA, 2014. EPA Positive Matrix Factorization (PMF) 5.0 - Fundamentals and user guide.  
1261 EPA/600/R-14/108  
1262
- 1263 Valotto, G., Squizzato, S., Masiol, M., Zannoni, D., Visin, F., Rampazzo, G., 2014. Elemental  
1264 characterization, sources and wind dependence of PM1 near Venice, Italy. *Atmos. Res.* 143, 371–  
1265 379.  
1266
- 1267 Wang, X., Zhang, Y., Chen, H., Yang, X., Chen, J., Geng, F., 2009. Particulate nitrate formation in  
1268 a highly polluted urban area: a case study by single-particle mass spectrometry in Shanghai.  
1269 *Environ. Sci. Technol.* 43, 3061-3066.  
1270
- 1271 Wegner, T., Hussein, T., Hämeri, K., Vesala, T., Kulmala, M. Weber, S., 2012. Properties of  
1272 aerosol signature size distributions in the urban environment as derived by cluster analysis. *Atmos.*  
1273 *Environ.* 61, 350-360.  
1274
- 1275 Wormhoudt, J., Herndon, S.C., Yelvington, P.E., Lye-Miake, R.C., Wey, C., 2007. Nitrogen oxide  
1276 (NO/NO<sub>2</sub>/HONO) emissions measurements in aircraft exhausts. *J. Propul. Power* 23, 906-911.  
1277
- 1278 Yue, W., Stölzel, M., Cyrys, J., Pitz, M., Heinrich, J., Kreyling, W.G., Wichmann, H.-E., Peters, A.,  
1279 Wang, S., Hopke, P.K., 2008. Source apportionment of ambient fine particle size distribution using  
1280 positive matrix factorization in Erfurt, Germany. *Sci. Total Environ.* 398, 133-144.

1281

1282 Zhang, K.M., Wexler, A.S., Zhu, Y.F., Hinds, W.C., Sioutas, C., 2004. Evolution of particle  
1283 number distribution near roadways. Part II: the 'Road-to-Ambient' process. *Atmos. Environ.* 38,  
1284 6655-6665.

1285

1286 Zhang, R., Khalizov, A., Wang, L., Hu, M., Xu, W., 2011. Nucleation and growth of nanoparticles  
1287 in the atmosphere. *Chem. Rev.* 112, 1957-2011.

1288

1289 Zhou, L., Kim, E., Hopke, P.K., Stanier, C.O. Pandis, S., 2004. Advanced factor analysis on  
1290 Pittsburgh particle size-distribution data special issue of aerosol science and technology on findings  
1291 from the Fine Particulate Matter Supersites Program. *Aerosol Sci. Technol.* 38(S1), 118-132.

1292

1293

1294

1295

1296

1297

ACCEPTED MANUSCRIPT

## TABLE LEGENDS

1298  
1299  
1300  
1301  
1302  
1303  
1304  
1305  
1306  
1307  
1308  
1309  
1310  
1311  
1312  
1313  
1314  
1315  
1316  
1317  
1318  
1319  
1320  
1321  
1322  
1323  
1324  
1325  
1326  
1327  
1328  
1329  
1330  
1331  
1332  
1333  
1334  
1335  
1336  
1337  
1338  
1339  
1340  
1341  
1342  
1343  
1344  
1345  
1346  
1347

**Table 1.** Summary of PMF analysis.

**Table 2.** Spearman's correlations among extracted factors, common air pollutants and some micro-meteorological parameters. Only correlations significant at  $p < 0.001$  are shown;  $\rho > 0.6$  are bold faced  $0.35 < \rho < 0.6$  are in italic.

**Table 3.** Results of wind sector analysis for BC data. Data have been filtered by wind speeds  $> 1 \text{ m s}^{-1}$ .

## FIGURE LEGENDS

**Figure 1.** Map of the study area (left): some local sources are highlighted by different colours. Detailed view of the airport of Venice (right): the sampling site is shown as a star.

**Figure 2.** a) Boxplots of some analysed pollutants (line= median, box= inter-quartile range, whiskers=  $\pm 1.5 \times$  inter-quartile range). b) Diurnal variations of levels of measured pollutants computed over the hourly averaged data during the sampling period (e.g., 6:00 refer to averaged data between 6:00 and 7:00). Each plot reports the average level as a filled line and the associated 75th and 99th confidence intervals calculated by bootstrapping the data ( $n=200$ ). In purple particle number data from SMPS and APS, which were roughly categorised as: nucleation (14-30 nm), Aitken nuclei (30 to 100 nm), accumulation (0.1 to 1  $\mu\text{m}$ ) and coarse particles (1 to 20  $\mu\text{m}$ ); in red gaseous pollutants; in black non-gaseous pollutants and in green some micro-meteorological variables. Data of airport traffic only refer to civil aviation movements.

**Figure 3.** Polar plots of analysed air pollutants. The position of the wind speed scale on each plot corresponds to the location of the runway. PNC and BC data were hourly-averaged to be matched with wind data.

**Figure 4.** Distributions particle number and volume categorised by daytime (01:00-07:00; 07:00-13:00; 13:00-19:00; 19:00-01:00 local time). Lines represent the median concentrations, while shaded areas report the 25th-75th percentile intervals.

**Figure 5.** Results of cluster analysis. Average cluster PNSD spectra (left) are reported as solid red lines along with: (i) their 10th, 25th, 75th and 90th percentile spectrum as shaded areas; (ii) the volume size distributions (dashed blue line); (iii) the hourly counts and (iv) the wind roses associated to each cluster.

**Figure 6.** Selected period (23th to 27th May). The plots represent (from upper to the bottom): (1) hourly counts of number of clusters; (2) airport traffic (arrivals+departures); (3) solar irradiation; (4) nitrogen oxide concentration; (5) sulphur dioxide concentration; (6) particle number concentration for the nucleation range (14-30 nm); (7) particle number concentration for the Aitken range (30-100 nm); (8) particle number concentration for the accumulation range (100-1000 nm); (9) BC concentration; (10) contour plots of SMPS data.

- 1348 **Figure 7.** Number (black solid line) and volume (red dashed line) distributions for the six  
1349 factors extracted by the PMF model. Data are expressed as normalised fractions on  
1350 the total from the final solution (FPEAK=2.5).  
1351
- 1352 **Figure 8.** Diurnal variations, polar plot and polar annulus of the six factors extracted from the  
1353 PMF model. Diurnal variations report the average level as a filled line and the  
1354 associated 75th and 99th confidence intervals calculated by bootstrapping the data  
1355 (n=200).  
1356
- 1357 **Figure 9.** Some CCFs computed among PMF factor contributions and other pollutants.  
1358
- 1359 **Figure 10.** a) Polarplot of BC (hourly averaged data) during the whole sampling campaign; b)  
1360 boxplots of the BC levels on filtered data for wind sectors and  $ws > 1 \text{ m s}^{-1}$  pollutants  
1361 (line= median, box= inter-quartile range, whiskers=  $\pm 1.5 \cdot$  inter-quartile range).

1362 **Table 1.** Summary of PMF analysis.

1363

No.	Most probable source	Main modes		Contributions		Peak hours (local time)	Significant correlations at $p < 0.001$ , $\rho > 0.35$ positive (negative)
		Dominant PNSD	PVSD	PNSD % (95th confidence interval)	PVSD %		
1	<b>Nucleation</b>	15-20 nm	200 nm; 2 $\mu\text{m}$	43.8 (43.4-44.1)	1.1	12am-1pm	NO, OX, solar irr., air temp.
2	<b>Traffic</b>	35-40 nm	80-90; 500 nm	25.5 (25.3-25.9)	4.8	6am-8am; 9pm-11pm	NO <sub>2</sub> , NO <sub>x</sub> , BC, (O <sub>3</sub> )
3	<b>Airport</b>	<14nm; 80 nm	200; 500 nm, 5 $\mu\text{m}$	20.3 (20.1-20.5)	19.6	–	–
4	<b>Nighttime nitrate</b>	30 nm; 200 nm	400 nm; 2.5 $\mu\text{m}$	5.9 (5.8-6.1)	41.2	5am-7am	NO <sub>2</sub> , BC, PM <sub>2.5</sub> , (O <sub>3</sub> ), (OX), (SO <sub>2</sub> ), (wind speed)
5	<b>Regional pollution</b>	60 nm	2-3 $\mu\text{m}$	3 (2.4-3.1)	21.1	12pm-6am	CO, PM <sub>2.5</sub>
6	<b>Local resuspension</b>	25 nm	5 $\mu\text{m}$	1.5 (1.3-1.6)	12.2	4am-6am	(O <sub>3</sub> ), (OX), (solar irr.), (air temp.), (wind speed)

1364

1365

1366

1367

1368

1369

1370

1371

1372

1373

1374



1375 **Table 2.** Spearman's correlations among extracted factors, common air pollutants and some micro-meteorological parameters. Only correlations  
 1376 significant at  $p < 0.001$  are shown;  $\rho > 0.6$  are bold faced  $0.35 < \rho < 0.6$  are in italic.

1377

Factors	CO	NO	NO <sub>2</sub>	NO <sub>x</sub>	O <sub>3</sub>	OX	SO <sub>2</sub>	BC	PM <sub>2.5</sub>	Wind speed	Air temp.	Solar irr.
<b>Factor 1: Nucleation</b>		<i>0.37</i>			0.31	<i>0.41</i>	0.33			0.20	<i>0.52</i>	<i>0.47</i>
<b>Factor 2: Traffic</b>	0.25		<i>0.44</i>	<i>0.41</i>	<i>-0.43</i>	-0.31	-0.23	<i>0.41</i>	0.19	-0.23	-0.22	
<b>Factor 3: Airport</b>	0.31	0.19						0.20				
<b>Factor 4: Nighttime nitrate</b>	0.31		<i>0.37</i>	0.33	<i>-0.53</i>	<i>-0.47</i>	<i>-0.43</i>	<b>0.64</b>	<i>0.48</i>	<i>-0.54</i>	-0.30	-0.17
<b>Factor 5: Regional pollution</b>	<i>0.52</i>				-0.30	-0.31	-0.39	0.29	<i>0.41</i>	-0.23	-0.33	-0.25
<b>Factor 6: Local resuspension</b>			0.24	0.20	<i>-0.55</i>	<i>-0.50</i>	-0.35	0.30	0.33	<i>-0.45</i>	<i>-0.54</i>	<i>-0.47</i>

1378

1379

1380

1381

1382

1383

1384

1385

1386

1387

1388

1389

1390

1391

1392

1393 **Table 3.** Results of wind sector analysis for BC data. Data have been filtered by wind speeds  $>1 \text{ m s}^{-1}$ .

1394

<b>Location</b>	<b>Sector</b>	<b>Mean<math>\pm</math>St.Dev.</b>	<b>Median (25th-75th percentile)</b>
	<i>degree</i>	$\mu\text{g m}^{-3}$	$\mu\text{g m}^{-3}$
<b>Urban area of Mestre</b>	240–280	1.0 $\pm$ 0.4	1 (0.8–1.2)
<b>Porto Marghera</b>	210–240	0.7 $\pm$ 0.3	0.7 (0.4–0.8)
<b>Venice</b>	170–210	0.8 $\pm$ 0.3	0.8 (0.7–1)
<b>Island of Murano</b>	150–170	0.8 $\pm$ 0.4	0.6 (0.6–0.9)
<b>VCE airfield</b>	30–150	0.7 $\pm$ 0.4	0.7 (0.5–0.9)
<b>Other directions</b>	280–30	1.5 $\pm$ 0.8	1.4 (0.9–1.9)

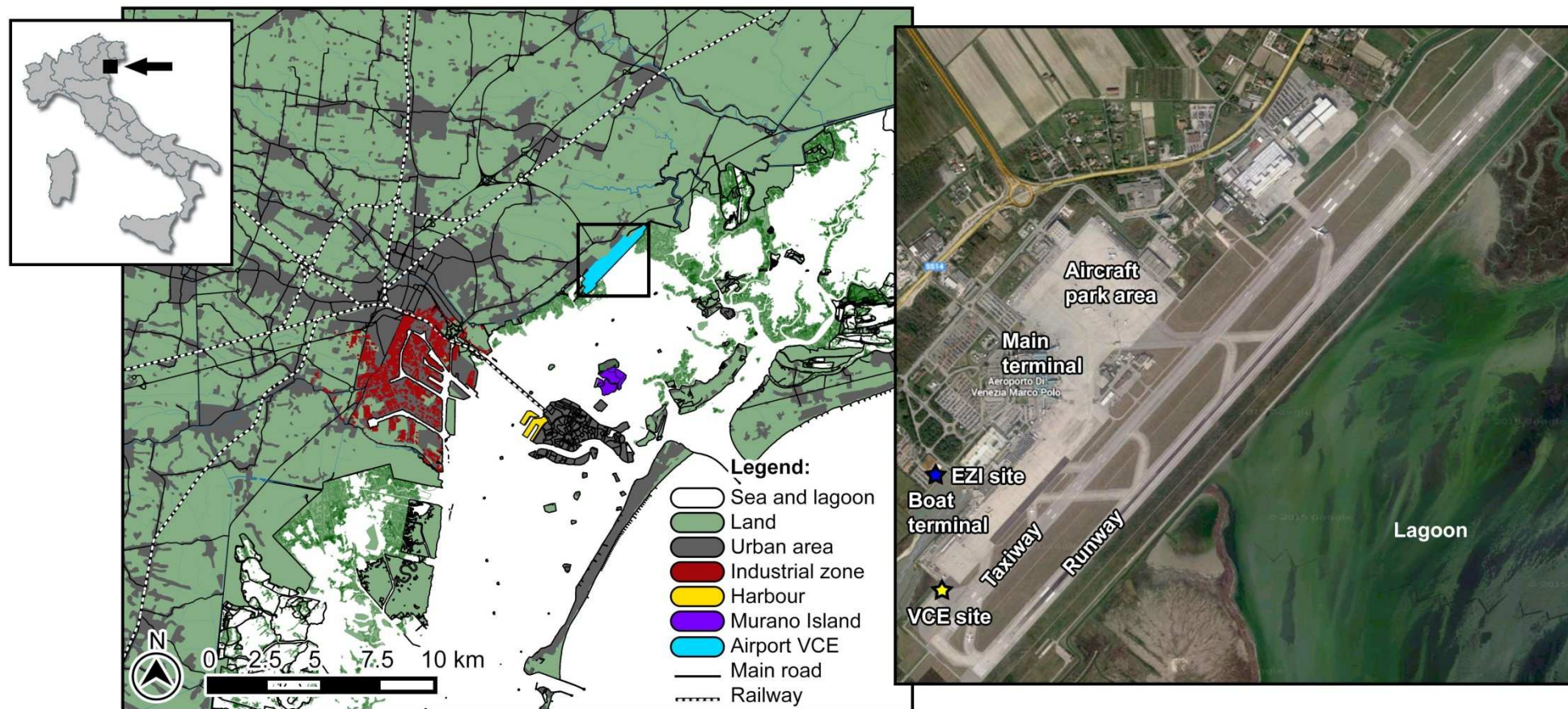
1395

1396

1397

1398

1399

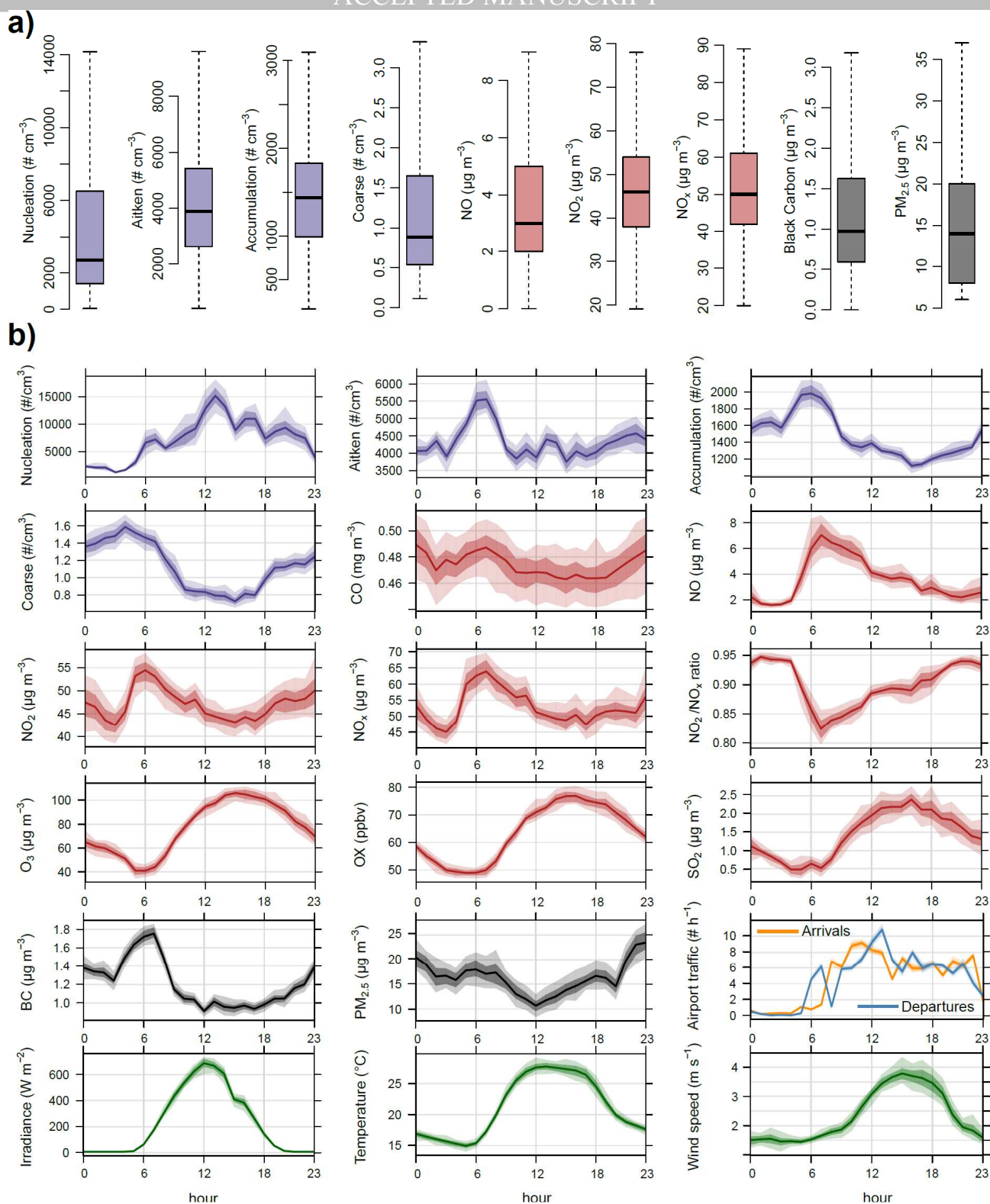


1400

1401

1402

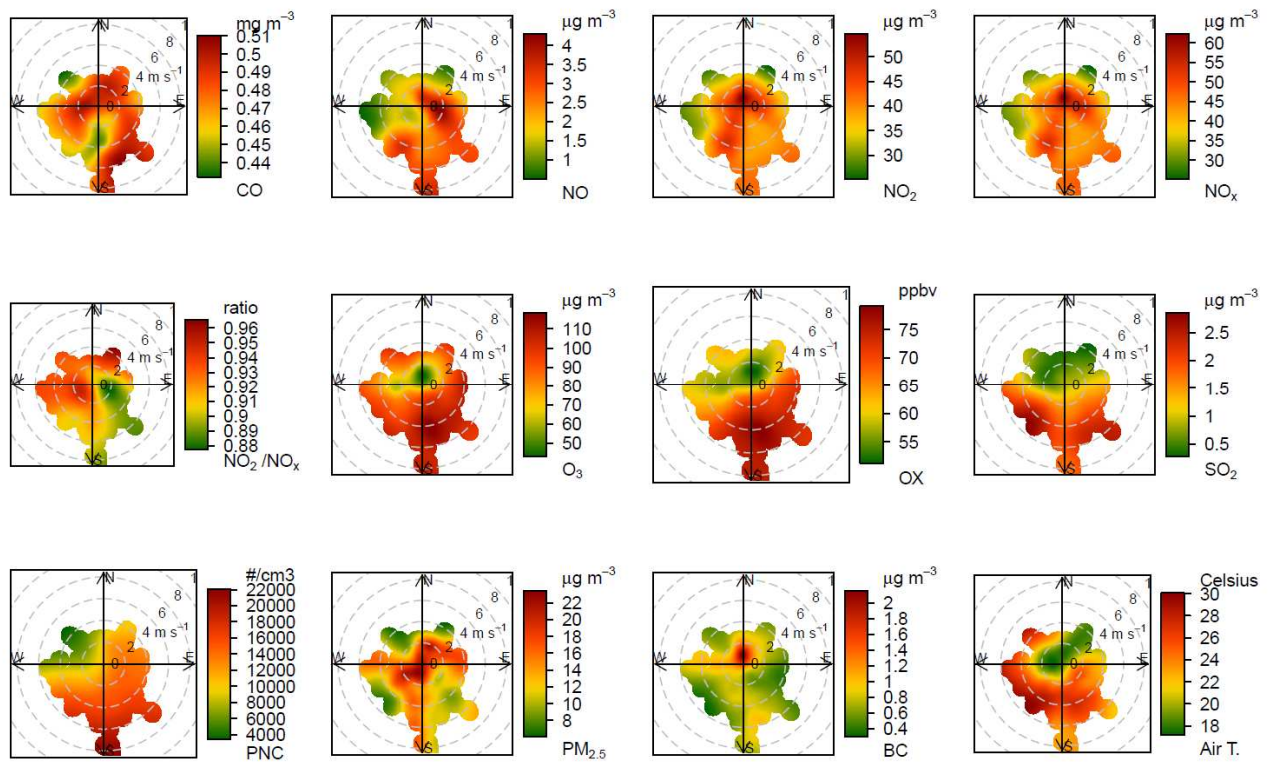
**Figure 1.** Map of the study area (left): some local sources are highlighted by different colours. Detailed view of the airport of Venice (right): the sampling site is shown as a star.



1403  
1404  
1405  
1406  
1407  
1408  
1409  
1410  
1411  
1412

**Figure 2.** a) Boxplots of some analysed pollutants (line= median, box= inter-quartile range, whiskers=  $\pm 1.5$ \*inter-quartile range). b) Diurnal variations of levels of measured pollutants computed over the hourly averaged data during the sampling period (e.g., 6:00 refer to averaged data between 6:00 and 7:00). Each plot reports the average level as a filled line and the associated 75th and 99th confidence intervals calculated by bootstrapping the data ( $n=200$ ). In purple particle number data from SMPS and APS, which were roughly categorised as: nucleation (14-30 nm), Aitken nuclei (30 to 100 nm), accumulation (0.1 to 1  $\mu\text{m}$ ) and coarse particles (1 to 20  $\mu\text{m}$ ); in red gaseous pollutants; in black non-gaseous pollutants and in green some micro-meteorological variables. Data of airport traffic only refer to civil aviation movements.

1413



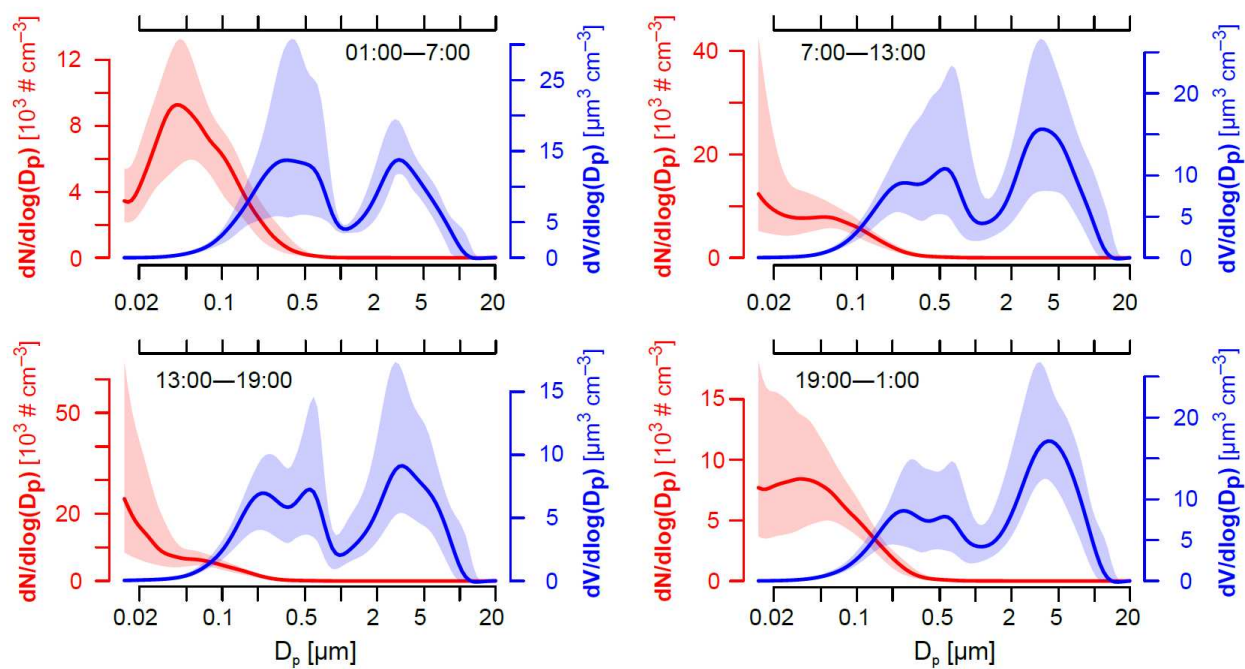
1414

1415 **Figure 3.** Polar plots of analysed air pollutants. The position of the wind speed scale on each plot  
 1416 corresponds to the location of the runway. PNC and BC data were hourly-averaged to be matched  
 1417 with wind data.

1418

1419

1420



1421

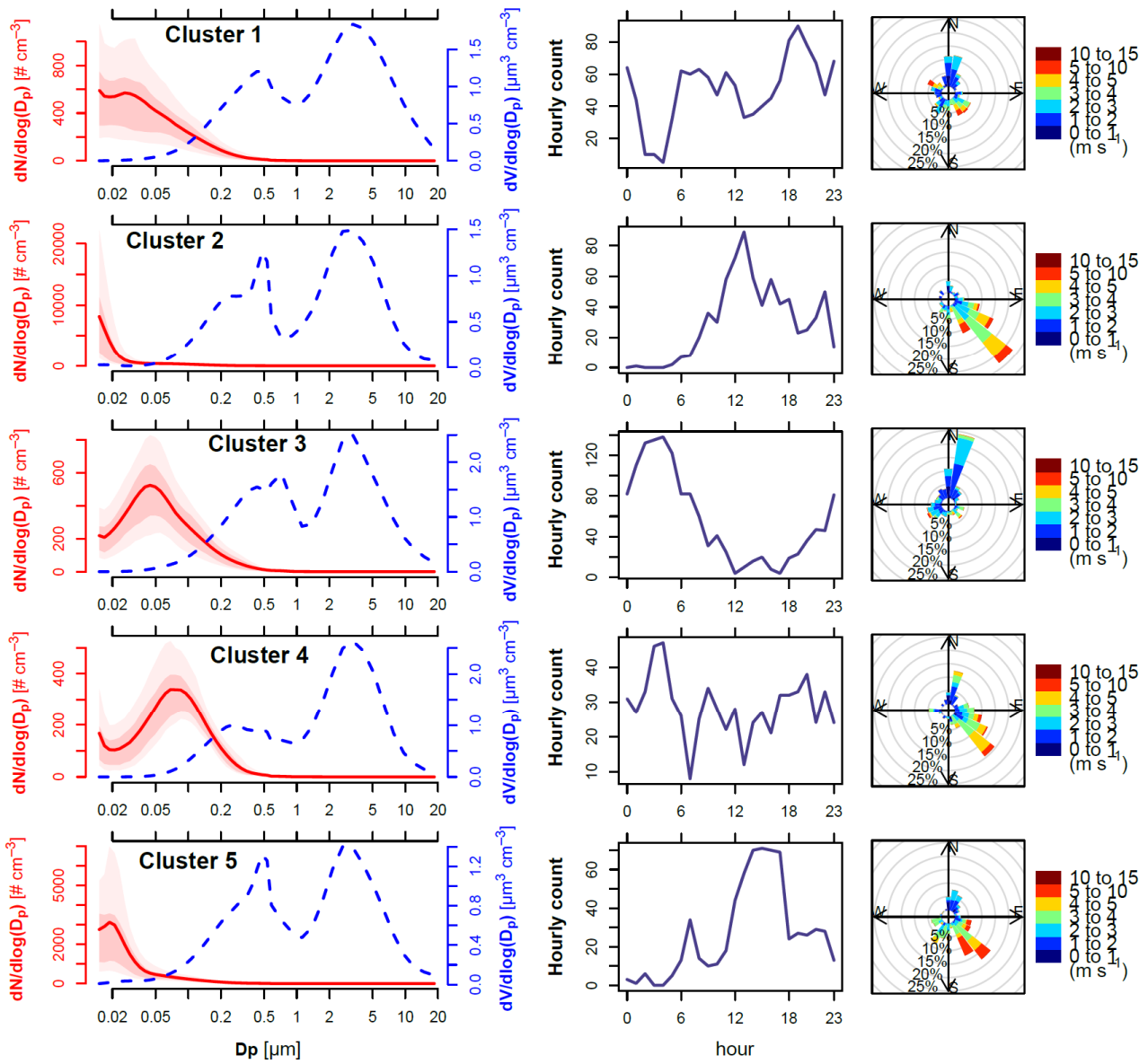
1422

1423

1424

1425

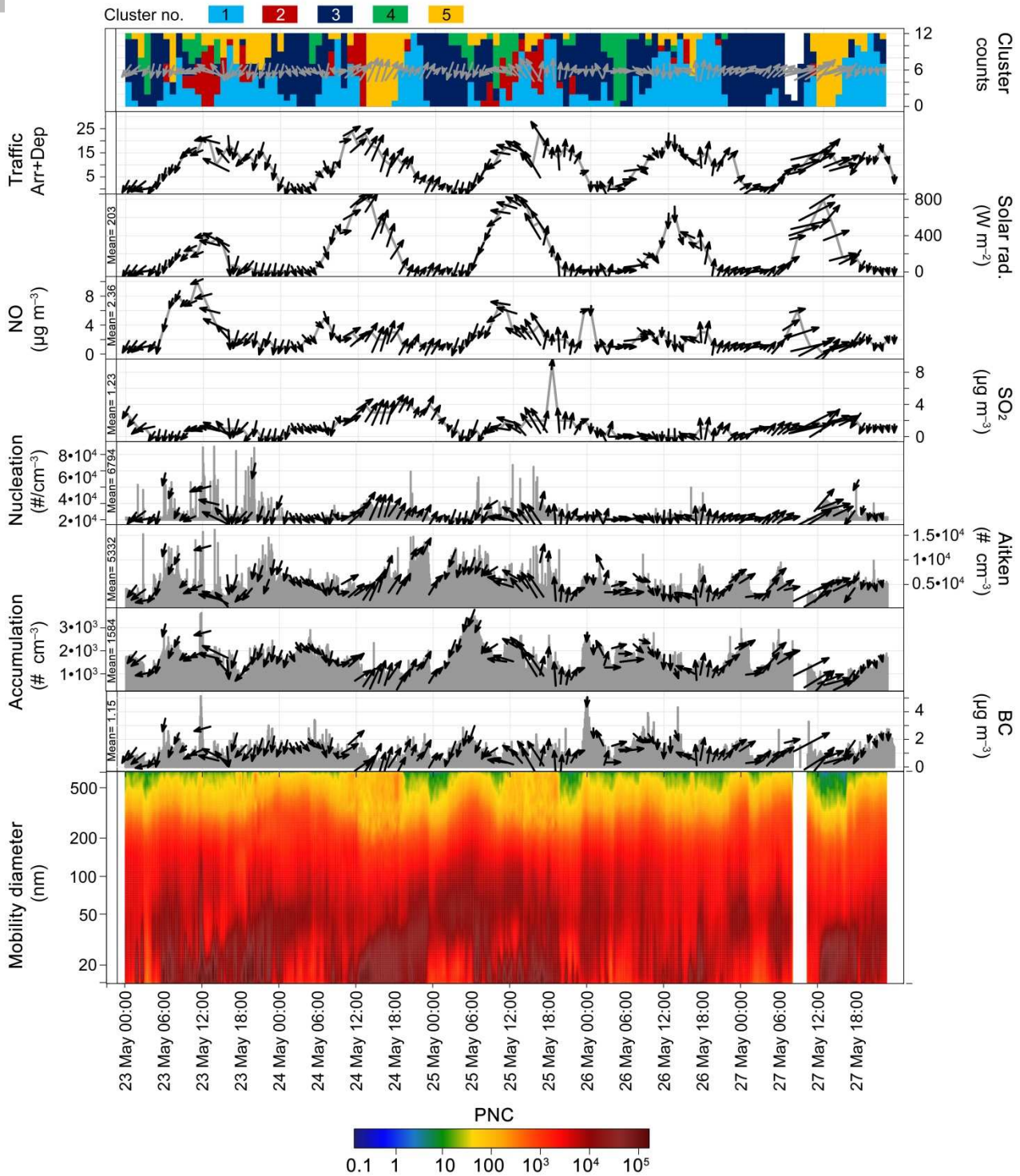
**Figure 4.** Distributions particle number and volume categorised by daytime (01:00-07:00; 07:00-13:00; 13:00-19:00; 19:00-01:00 local time). Lines represent the median concentrations, while shaded areas report the 25th-75th percentile intervals.



1426

1427 **Figure 5.** Results of cluster analysis. Average cluster PNSD spectra (left) are reported as solid red  
 1428 lines along with: (i) their 10th, 25th, 75th and 90th percentile spectrum as shaded areas; (ii) the  
 1429 volume size distributions (dashed blue line); (iii) the hourly counts and (iv) the wind roses  
 1430 associated to each cluster.

1431



1432

1433

1434

1435

1436

1437

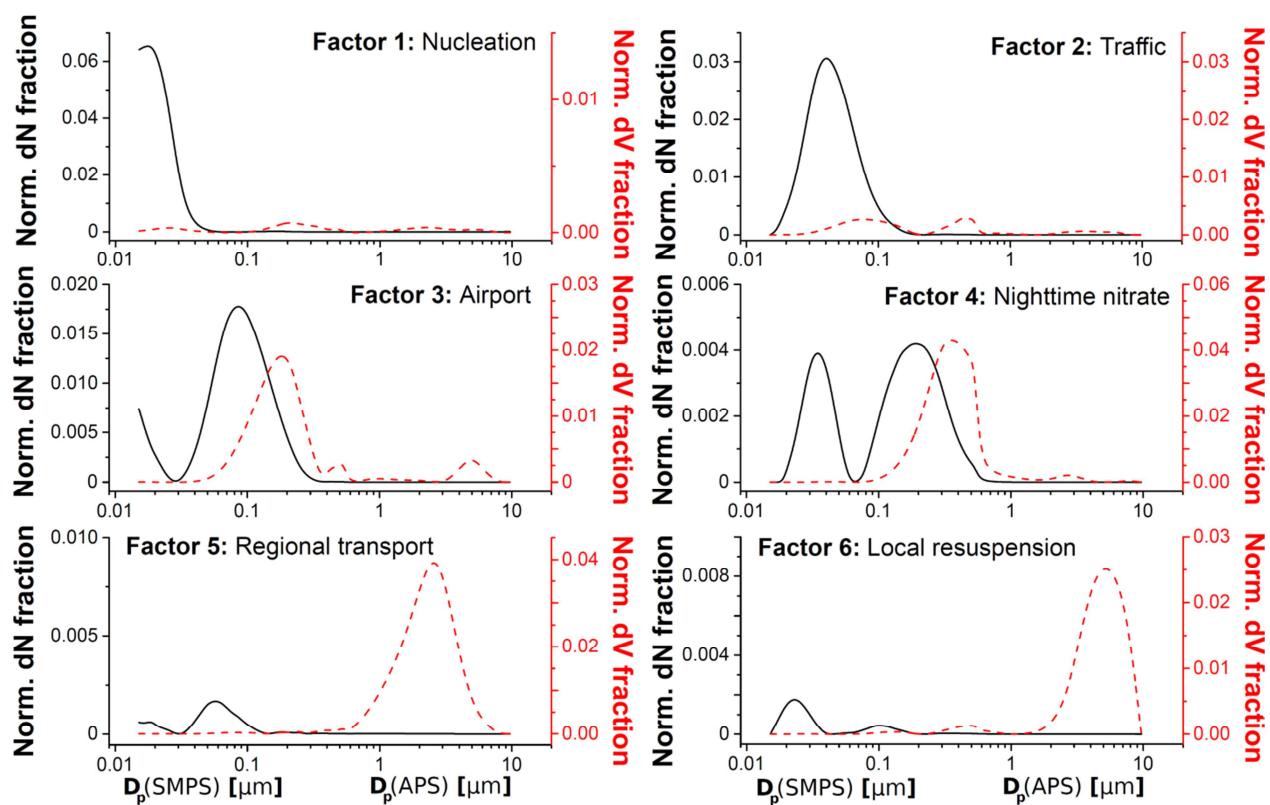
1438

**Figure 6.** Selected period (23th to 27th May). The plots represent (from upper to the bottom): (1) hourly counts of number of clusters; (2) airport traffic (arrivals+departures); (3) solar irradiation; (4) nitrogen oxide concentration; (5) sulphur dioxide concentration; (6) particle number concentration for the nucleation range (14-30 nm); (7) particle number concentration for the Aitken range (30-100 nm); (8) particle number concentration for the accumulation range (100-1000 nm); (9) BC concentration; (10) contour plots of SMPS data.



1439

1440



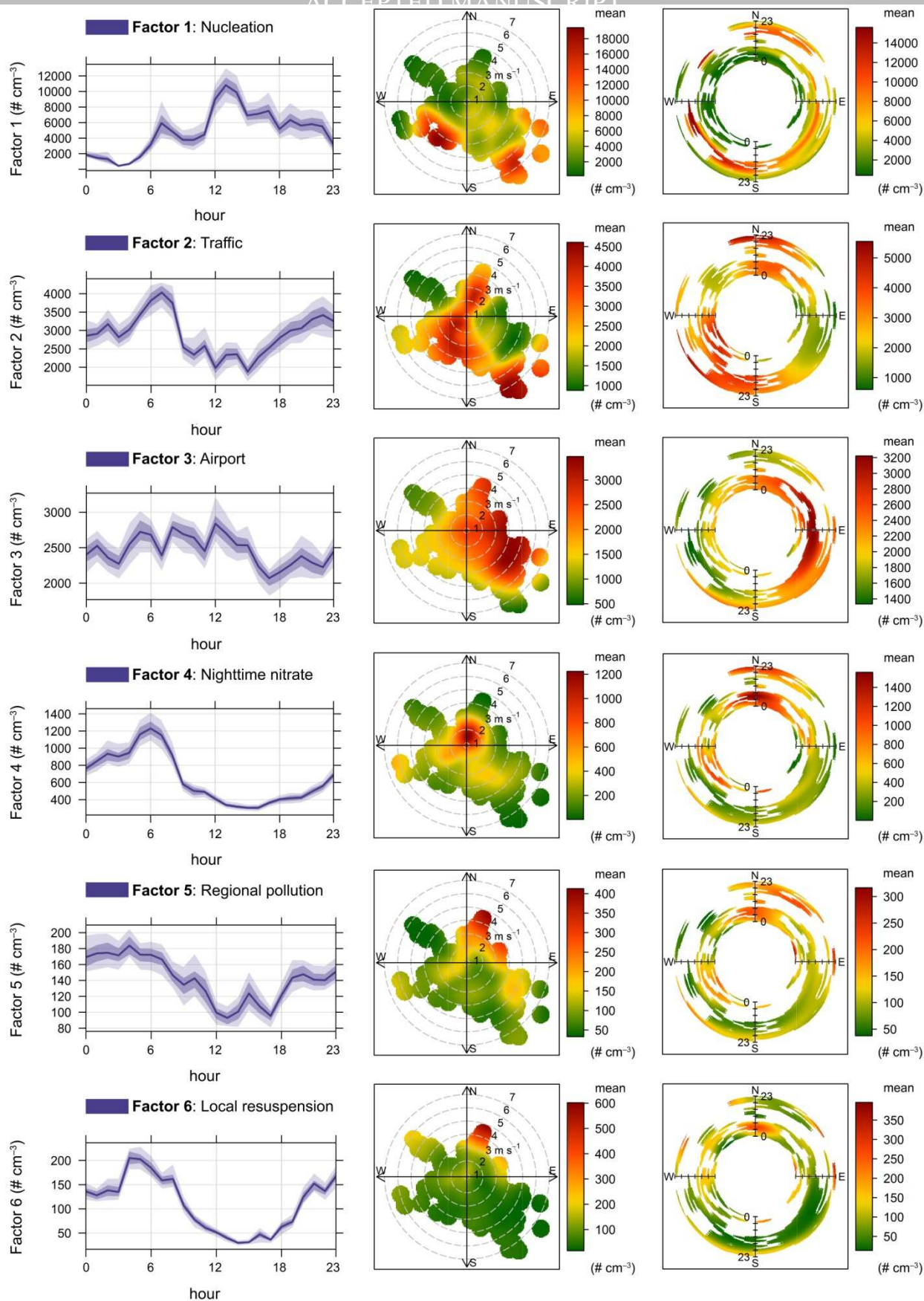
1441

1442

1443 **Figure 7.** Number (black solid line) and volume (red dashed line) distributions for the six factors  
 1444 extracted by the PMF model. Data are expressed as normalised fractions on the total from the final  
 1445 solution (FPEAK=2.5).

1446

1447



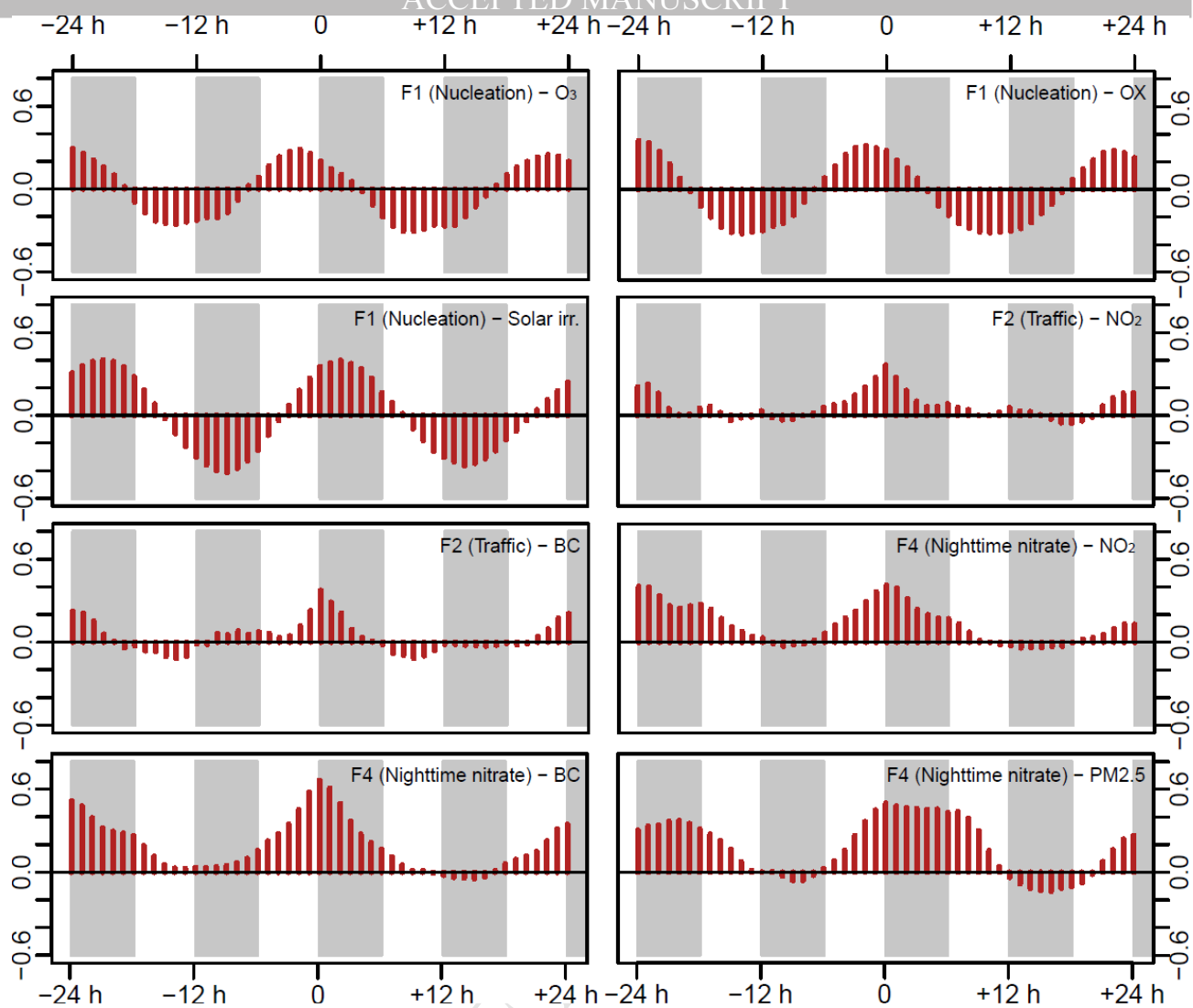
1448

1449

1450

1451

**Figure 8.** Diurnal variations, polar plot and polar annulus of the six factors extracted from the PMF model. Diurnal variations report the average level as a filled line and the associated 75th and 99th confidence intervals calculated by bootstrapping the data (n=200).



1452

1453

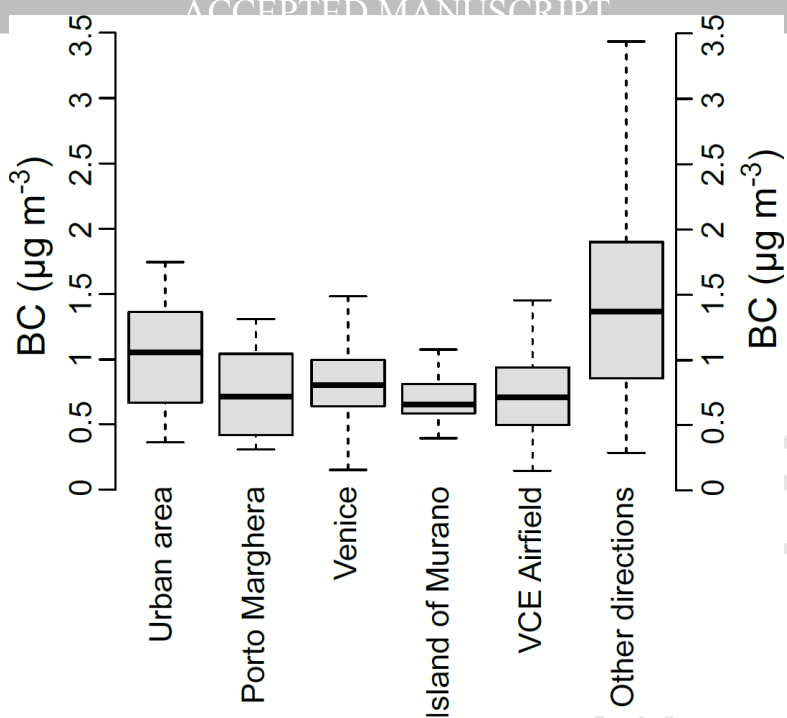
1454 **Figure 9.** Some CCFs computed among PMF factor contributions and other pollutants.

1455

1456

1457

1458



1459

1460

1461

1462

**Figure 10.** a) Polarplot of BC (hourly averaged data) during the whole sampling campaign; b) boxplots of the BC levels on filtered data for wind sectors and  $ws > 1 \text{ m s}^{-1}$  pollutants (line= median, box= inter-quartile range, whiskers=  $\pm 1.5$ \*inter-quartile range).